LETTER

doi:10.1038/nature22067

Human umbilical cord plasma proteins revitalize hippocampal function in aged mice

Joseph M. Castellano[1,2], Kira I. Mosher[1,2,3], Rachelle J. Abbey[1,2,4], Alisha A. McBride[1,2,4], Michelle L. James[1,5], Daniela Berdnik[1,2,4], Jadon C. Shen[1,2,4], Bende Zou[6], Xinmin S. Xie[6,7], Martha Tingle[7], Izumi V. Hinkson[1,2,4], Martin S. Angst[7] & Tony Wyss-Coray[1,2,3,4]

Ageing drives changes in neuronal and cognitive function, the decline of which is a major feature of many neurological disorders. The hippocampus, a brain region subserving roles of spatial and episodic memory and learning, is sensitive to the detrimental effects of ageing at morphological and molecular levels. With advancing age, synapses in various hippocampal subfields exhibit impaired long-term potentiation[1], an electrophysiological correlate of learning and memory. At the molecular level, immediate early genes are among the synaptic plasticity genes that are both induced by long-term potentiation[2–4] and downregulated in the aged brain[5–8]. In addition to revitalizing other aged tissues[9–13], exposure to factors in young blood counteracts age-related changes in these central nervous system parameters[14–16], although the identities of specific cognition-promoting factors or whether such activity exists in human plasma remains unknown[17]. We hypothesized that plasma of an early developmental stage, namely umbilical cord plasma, provides a reservoir of such plasticity-promoting proteins. Here we show that human cord plasma treatment revitalizes the hippocampus and improves cognitive function in aged mice. Tissue inhibitor of metalloproteinases 2 (TIMP2), a blood-borne factor enriched in human cord plasma, young mouse plasma, and young mouse hippocampi, appears in the brain after systemic administration and increases synaptic plasticity and hippocampal-dependent cognition in aged mice. Depletion experiments in aged mice revealed TIMP2 to be necessary for the cognitive benefits conferred by cord plasma. We find that systemic pools of TIMP2 are necessary for spatial memory in young mice, while treatment of brain slices with TIMP2 antibody prevents long-term potentiation, arguing for previously unknown roles for TIMP2 in normal hippocampal function. Our findings reveal that human cord plasma contains plasticity-enhancing proteins of high translational value for targeting ageing- or disease-associated hippocampal dysfunction.

To begin to characterize differences in plasma proteins during different periods of life, we measured 66 common proteins in blood plasma from elderly individuals (aged 61–82 years), young adults (aged 19–24 years), and umbilical cord plasma from neonates (Extended Data Fig. 1a). Unsupervised clustering revealed distinct separation by age group in plasma proteins (Extended Data Fig. 1b). Proteins expected to be elevated in cord plasma, including human chorionic gonadotropin-β and α-fetoprotein, were increased (Extended Data Fig. 1c, d), and we detected age-related increases in immunoglobulin M (Extended Data Fig. 1e). To assess whether human plasma alters the hippocampus, a brain region critical for memory and influenced by young blood[15,16], we used immunodeficient 'NOD/SCID' (NSG) mice that could receive intravenous infusions of human plasma without adverse immune consequences[18]. Immunohistochemical comparison of hippocampi from young and aged NSG mice revealed reduced activation of the synaptic plasticity marker c-Fos, impaired neurogenesis, and increased microgliosis with age (Extended Data Fig. 2a–f), consistent with observations in wild-type (WT) mice[15,16,19]. Compared with young NSG mice, aged mice exhibited impaired hippocampal-dependent learning and memory performance (Extended Data Fig. 2g–l) in modified Barnes maze[20] and contextual fear-conditioning tests; these differences were unrelated to pain, visual, and auditory sensory function (Extended Data Fig. 2m–p). Thus, NSG mice exhibit typical age-related hippocampal dysfunction observed in WT mice by Barnes maze (Extended Data Fig. 2q, r) and fear-conditioning[15], seemingly at an earlier age.

To assess whether human cord plasma revitalizes aspects of brain function, plasma pools were created from cord, young adult, and elderly donors and injected intravenously into aged NSG mice every fourth day for 2 weeks before dissection of hippocampi for analyses (Fig. 1a). Whole-genome microarray analysis revealed transcriptional profiles from hippocampi that distinctly clustered by intravenous treatment (Fig. 1b); the groups separated across the first three principal components, explaining the most gene expression variance (Fig. 1c). Ontology-based comparison analysis of differentially expressed genes in human plasma- or vehicle-treated hippocampi suggested increased long-term potentiation (LTP) as a result of cord (Z-score = 2.12; $P = 2.68 \times 10^{-2}$) or young (Z-score = 0.96; $P = 2.59 \times 10^{-3}$) treatment, but not elderly ($P > 0.05$) plasma treatment. An additional predicted disease and functional pathway was memory (Z-score = 1.38; $P = 2.61 \times 10^{-2}$), although only as a result of cord plasma treatment. The immediate early gene (IEG) *cFos* (also known as *Fos*) was among the top three most significantly increased genes resulting from cord plasma treatment, suggesting a possible re-activation of genes linked to memory consolidation[1,21,22]. To confirm the induction of IEGs and other genes linked to plasticity and memory, we measured gene expression by quantitative (q)PCR in dissected hippocampi from treated mice, finding that cord plasma treatment significantly increased expression of *Egr1*, *Junb*, *Camk2a*, *Bdnf*, *Ntf3*, *Ppp3ca*, *cFos*, and *Nptx2*, a late-response c-Fos/Junb target gene[22] (Fig. 1d). Notably, young adult human plasma treatment increased expression in a smaller subset of these genes, while elderly plasma did not lead to significant changes (Extended Data Fig. 3a, b). At the protein level, only cord plasma treatment significantly increased the number of c-Fos-expressing cells within aged dentate gyrus (Fig. 1e and Extended Data Fig. 3c). The activation seemed to depend on context, since the pattern was not observed in other regions, including amygdala and motor cortex (Extended Data Fig. 3d, e), nor was it observed in young hippocampi (Fig. 1f). Human plasma treatments did not alter phosphorylated cyclic AMP responsive element-binding protein (CREB)[16] or hippocampal neurogenesis (Extended Data Fig. 3f–i), possibly because neural stem cells are depleted in the aged NSG brain. We next used the targeted recombination in active populations

[1]Department of Neurology and Neurological Sciences, Stanford University School of Medicine, Stanford, California 94305, USA. [2]Paul F. Glenn Center for the Biology of Aging, Stanford University School of Medicine, Stanford, California 94305, USA. [3]Neuroscience Graduate Program, Stanford University School of Medicine, Stanford, California 94305, USA. [4]Center for Tissue Regeneration, Repair and Restoration, V.A. Palo Alto Healthcare System, Palo Alto, California 94304, USA. [5]Molecular Imaging Program at Stanford, Radiology, Stanford University School of Medicine, Stanford, California 94305, USA. [6]AfaSci Research Laboratories, Redwood City, California 94063, USA. [7]Department of Anesthesiology, Perioperative and Pain Medicine, Stanford University School of Medicine, Stanford, California 94305, USA.

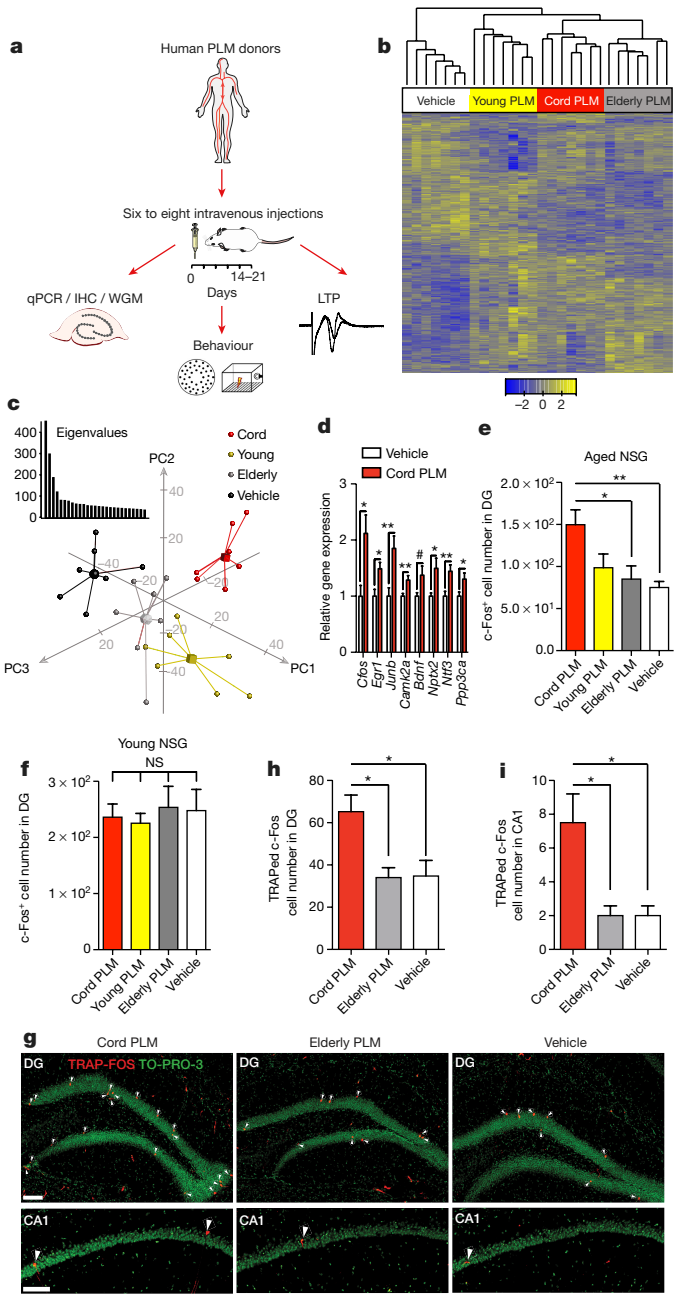

Figure 1 | Human cord plasma enhances plasticity in the aged brain. a, Human plasma (PLM) transfer protocol in aged NSG mice. **b**, Heat map of unsupervised clustering of gene changes in hippocampi following human plasma treatment of aged NSG mice ($n = 7$ per group; 13.8 ± 0.2 months old; colour bar represents Z-score range; one-way analysis of variance (ANOVA); $P < 0.05$). **c**, Three-dimensional plot of the first three components from PCA of whole-genome microarrays (WGM); inset graph represents eigenvalues (y axis) plotted against component number (x axis). **d**, Relative gene expression by qPCR for confirmatory plasticity genes after vehicle or human cord plasma treatment ($n = 7$ per group; 13.9 ± 0.2 months old). **e**, **f**, c-Fos-positive cell number in dentate gyrus (DG) of human-plasma-treated aged (**e**; $n = 8, 7, 7, 7$ mice per group (left to right); 13.9 ± 0.2 months old) or young (**f**) NSG mice ($n = 8$ mice per group; 3.4 ± 0.1 months old). **g**, Representative dentate gyrus and CA1 images and (**h**, **i**) recombined cell quantification (red; TdTomato) with counterstain (green; TO-PRO-3) from treated TRAP-FOS mice ($n = 4, 3, 4$ mice per group (left to right); 8–9.5 months old; scale bar, 100 μm). One-way ANOVA with Tukey's post hoc test; Student's t-test for two-group comparisons; $^*P < 0.05$, $^{**}P < 0.01$, $\#P = 0.05$; mean ± s.e.m.

(TRAP-FOS) model[23] to assess whether cord-plasma-mediated plasticity changes are observed in WT mice, yet without immune activation resulting from repeated human plasma injections. Given the striking effects following cord plasma but not other plasma treatments, we treated TRAP-FOS mice (C57Bl/6J background) with cord, vehicle, and elderly plasma (as plasma control). In the presence of tamoxifen and sufficient stimulus, *fos*-active cells are permanently visualized by tdTomato effector expression[23]. Three days after a single injection of cord plasma, significantly more c-Fos-TRAPed cells were detected in the dentate gyrus and CA1 subfield (Fig. 1g–i and Extended Data Fig. 3j, k), but not other regions (Extended Data Fig. 3l, m), compared with control-injected mice. These results suggest cord plasma activates neuronal activity in the context of a functional immune system.

Given that dentate gyrus cells activated by cord plasma were granule-cell excitatory neurons[24] (Extended Data Fig. 4a–e), and that neuronal c-Fos induction is important for synaptic plasticity underlying learning and memory[2,21,22], we measured LTP in hippocampal slices from a separate cohort of aged NSG mice treated with cord plasma or vehicle. Extracellular recordings in dentate gyrus synapses revealed that cord plasma treatments significantly increased LTP compared with vehicle (Fig. 2a–c), although synaptic strength and paired-pulse facilitation were unaffected (Extended Data Fig. 5a–c), suggesting a postsynaptic mechanism. The effect on LTP was not observed in slices from young NSG mice treated with cord plasma (Extended Data Fig. 5d–f). Neither elderly nor young plasma treatment in aged NSG mice significantly affected LTP, although the latter treatment produced a trend towards increased LTP (Extended Data Fig. 5g–i). To corroborate improvements observed in cognition-linked molecular and cellular plasticity parameters, we subjected separate cohorts of treated aged mice to Barnes maze and fear-conditioning testing. Cord-plasma-treated aged NSG mice reached the escape hole with

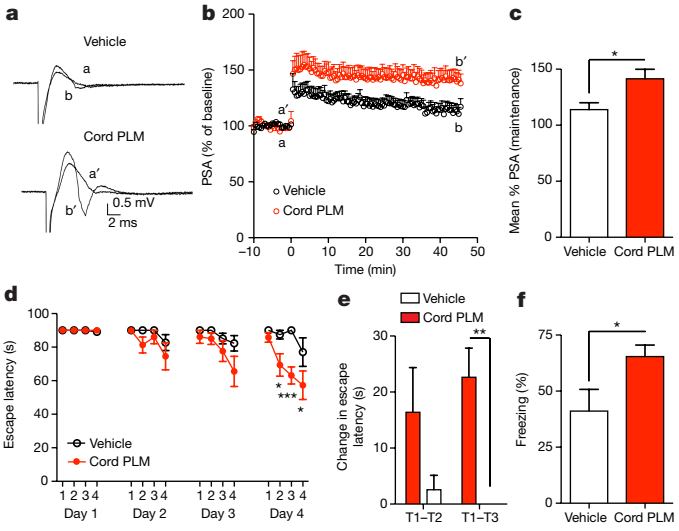

Figure 2 | Cord plasma improves neuronal function within aged hippocampus. a, **b**, Population spike amplitudes recorded in dentate gyrus granule cell layer by perforant path stimulation with representative traces before LTP induction (a/a′) and after LTP maintenance (b/b′) ($n = 11$–12 slices per group (see Source Data for range details) from $n = 5$ NSG mice per group; eight intravenous injections; 11.7 ± 0.2 months old). **c**, LTP maintenance-phase quantification. **d**, Days 1–4 escape latency and (**e**) fourth-day acquisition rate of cord-plasma-treated ($n = 8$) or vehicle-treated ($n = 7$) NSG mice in Barnes maze (eight intravenous injections; 12.9 ± 0.2 months old); T, trial. **f**, Contextual fear-conditioning freezing levels in separate cohort of cord-plasma-treated ($n = 7$) or vehicle-treated ($n = 9$) NSG mice (eight intravenous injections; 12.8 ± 0.2 months old). Two-way repeated-measures ANOVA with Bonferroni's post hoc test for time × group comparisons; Student's t-test for two-group comparisons. $^*P < 0.05$, $^{**}P < 0.01$, $^{***}P < 0.001$; mean ± s.e.m.

shorter latency on the final testing day compared with vehicle-treated mice (Fig. 2d), and their acquisition rate was faster (Fig. 2e). Moreover, despite no differences in baseline freezing or cued freezing (Extended Data Fig. 5j, k), freezing levels during the hippocampal-dependent contextual memory task were significantly higher in cord-plasma-treated mice (Fig. 2f). Together, these results are consistent with predicted cord-plasma-mediated LTP and memory activations from ontology-based analysis of whole-genome microarrays.

Since cord plasma appeared to possess potent plasticity-promoting factors, we examined relative plasma protein changes in human donor groups and compared them with those in mouse plasma. We used customized discovery protein microarrays to detect several hundred plasma proteins of diverse functional classes (Supplementary Table 1). Unsupervised hierarchical clustering revealed age-dependent separation of changes in human and mouse plasma proteins (Fig. 3a). We thus created a youth-associated protein list by overlapping human and mouse age-related plasma changes and by examining changes in aged mice after sharing young blood via parabiosis[16] (Extended Data Fig. 6a). We treated aged C57Bl/6 (WT) mice systemically with recombinant versions of several top candidate proteins. Treatment with CSF2 and TIMP2, but not GAS6, increased c-Fos activation in the dentate gyrus (Fig. 3b). Cord-plasma-enriched CSF2 improved hippocampal-dependent memory in aged mice (Extended Data Fig. 6b–k), consistent with previous work in aged mice that develop Alzheimer's disease pathology[25] and validating our screening approach. Given the unexplored role of TIMP2 in CNS plasticity and cognition, we further pursued TIMP2 and confirmed elevations in cord plasma by enzyme-linked immunosorbent assay (ELISA) (Fig. 3c). Elevations were also observed between 7- to 8-week-old and 20-month-old mouse plasma by immunoblotting—differences that were larger between very young (1-month-old) and 20-month-old mice (Fig. 3d, e and Extended Data Fig. 7a, b). Importantly, the 21- to 22-kDa TIMP2 band was absent in young TIMP2 knockout (KO) plasma (Fig. 3d). We detected an age-related decline in TIMP2 protein in hippocampal lysates by immunoblotting (Extended Data Fig. 7c, d). Using confocal microscopy to further dissect changes in hippocampal TIMP2, we again found an age-related decline in TIMP2, most strikingly in neurons of the subgranular zone and hilar areas of dentate gyrus using a TIMP2 antibody validated in knockout sections (Fig. 3f and Extended Data Fig. 7e–h). The decline in TIMP2 may be related not to changes in overall intensity but rather to a gradual age-related loss of neurons within this subregion (Extended Data Fig. 7i, j).

Using doses of 25–100 $\mu g\,kg^{-1}$, we injected aged WT mice once or four times and examined c-Fos expression. Four TIMP2 injections every other day at 50 $\mu g\,kg^{-1}$ were needed to elicit significant c-Fos activation (Extended Data Fig. 7k, l). ^{64}Cu-radiolabelled TIMP2 injected at this dose was detected in brain at significantly higher levels than albumin control and persisted 24 h after injection, while blood TIMP2 levels declined (Fig. 3g, h and Extended Data Fig. 7m, n). Importantly, high-performance liquid chromatography in brain lysates of injected mice revealed a single radiolabelled species corresponding to the elution profile of intact TIMP2 before injection (Extended Data Fig. 7p, q). Autoradiography revealed substantial entry into ventricular spaces approximately 24 h after ^{64}Cu-labelled TIMP2 injection, as well as signal in parenchyma, albeit to a lesser extent (Extended Data Fig. 7o). To assess whether 50 $\mu g\,kg^{-1}$ TIMP2 activates c-Fos under conditions of physiological neuronal activity, we allowed mice to explore an enriched, novel environment. Enriched arena exploration alone activated c-Fos in dentate gyrus relative to normal housing conditions (Fig. 3i), but arena-enriched mice also treated with TIMP2 exhibited a potentiated c-Fos response, suggesting that systemic TIMP2 activates plasticity under conditions of normal hippocampal function.

To investigate whether systemic TIMP2 was sufficient to improve hippocampal-dependent learning and memory, we administered TIMP2 over 2 weeks, leading to significant improvements in several functional outcomes (Extended Data Fig. 7r and Fig. 4a–f). TIMP2

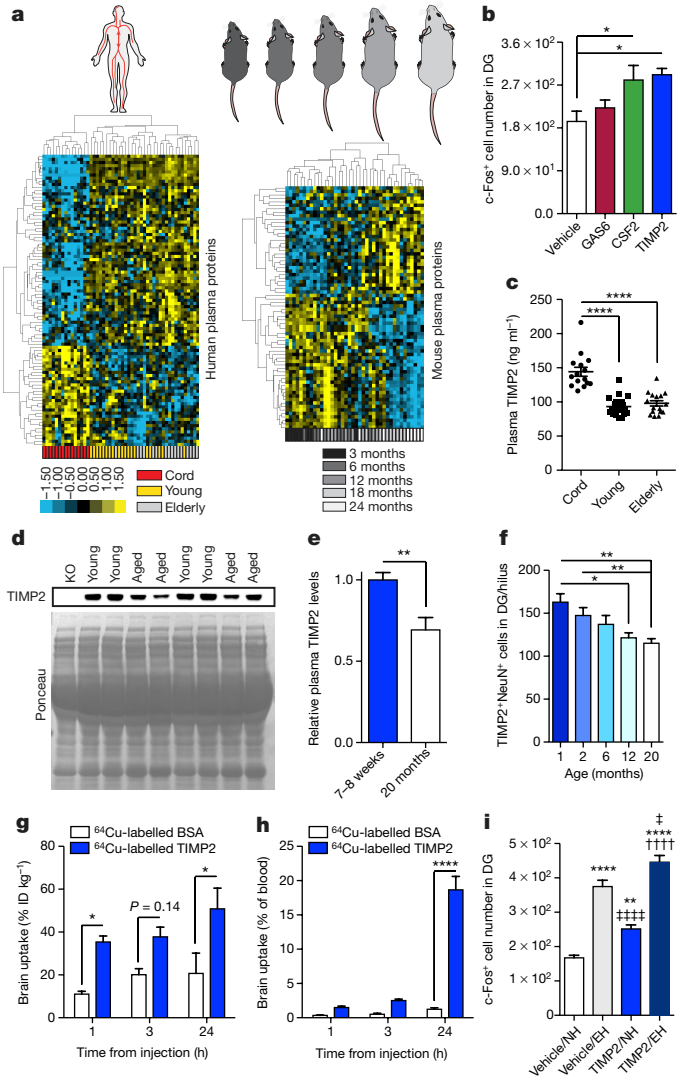

Figure 3 | Protein microarray analysis identifies putative pro-plasticity factors. a, Heat maps from unsupervised hierarchical cluster analysis of human ($n = 15$ cord, 19 young, 16 elderly subjects; $|d\text{-score}| \geq 1.30$) or mouse ($n = 8$ mice per group; 3, 6, 12, 18, and 24 months of age; $|d\text{-score}| \geq 1.3$) plasma protein changes analysed by significance analysis of microarray (SAM) for quantitative ageing correlations. Relative Z-scored values indicated in graded yellow (high) or blue (low). **b**, Number of c-Fos-positive cells in dentate gyrus from aged (16-month-old) WT mice treated four times every other day with 50 $\mu g\,kg^{-1}$ (intraperitoneal) recombinant GAS6, CSF2, or TIMP2 or vehicle ($n = 6$ mice per group). **c**, ELISA-based plasma TIMP2 measurements from subjects in **a**. **d**, **e**, Representative TIMP2 immunoblot from equal volumes of 7- to 8-week-old or 20-month-old WT mouse plasma with corresponding Ponceau S stain (**d**) and quantification (**e**; $n = 8$ per group); see Supplementary Fig. 1 for uncropped image. **f**, Quantification of TIMP2$^+$ cells with NeuN$^+$ nuclei in dentate gyrus (hilus) by confocal microscopy of WT mice at indicated ages ($n = 8, 8, 6, 8, 9$ mice per group (left to right)). **g**, **h**, Brain uptake of ^{64}Cu-labelled bovine serum albumin (BSA) ($n = 4$ mice per time point ($n = 3$ at 24 h)) and TIMP2 ($n = 5$ mice per time point) in WT mice (21-month-old) euthanized at indicated time points after injected (intraperitoneal) tracer dose (ID; **g**) and as a proportion of tracer remaining in blood (**h**). **i**, c-Fos-positive cell counts within dentate gyrus from WT mice in normal housing (NH) or enriched housing (EH) injected four times with vehicle or TIMP2 ($n = 8, 8, 8, 7$ per group (left to right); 20-month-old; *versus vehicle/normal housing; ‡versus vehicle/enriched housing; †versus TIMP2/normal housing). One-way ANOVA with Tukey's post hoc test (Dunnett's in **b**); two-way ANOVA with Bonferroni's post hoc test for group × time comparisons; Student's t-test for two-group comparisons; one, two, or four symbols denote $P < 0.05$, 0.01, 0.0001, respectively; mean ± s.e.m. Mouse schematic adapted from ref. 16.

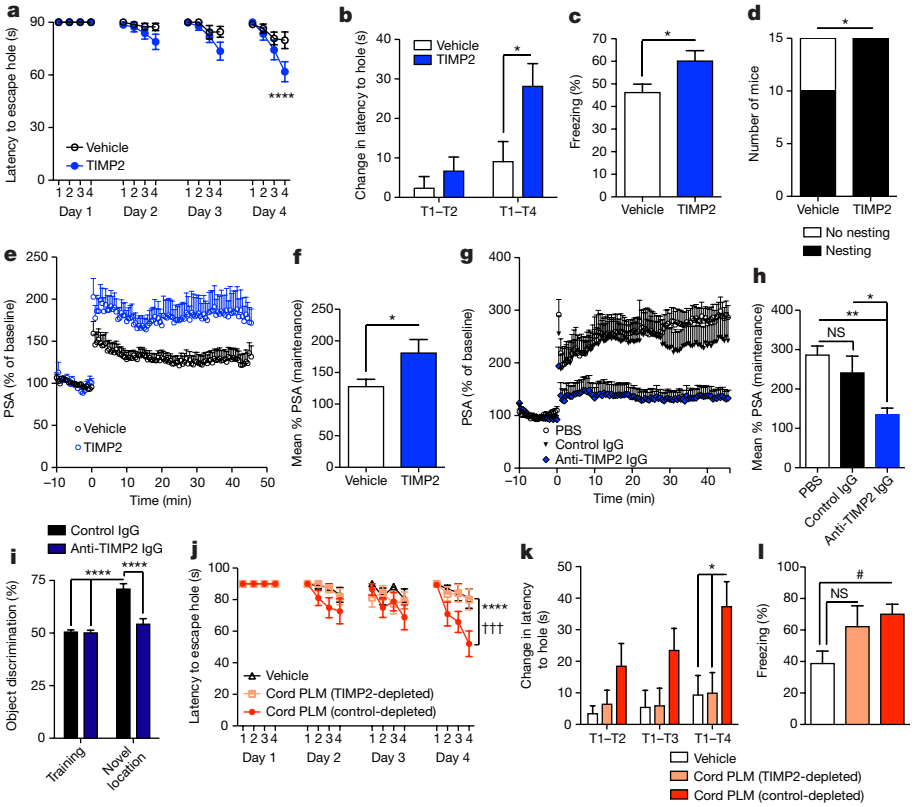

Figure 4 | Systemic TIMP2 treatment improves neuronal function within aged hippocampus and is critical for normal spatial memory and cognitive effects of cord plasma. a–d, Barnes maze escape latency for all trial days (**a**), fourth-day acquisition rate (**b**), freezing levels during contextual fear-conditioning (**c**), and nesting behaviour within 24 h of providing intact nestlet (**d**) for aged WT mice given eight systemic vehicle or TIMP2 injections every other day ($n = 15$ per group; 20-month-old). **e**, **f**, Population spike amplitudes recorded in dentate gyrus granule cell layer following perforant path stimulation (**e**) and maintenance-phase LTP quantification (**f**; $n = 10$ slices per group from $n = 5$ mice per group; eight intravenous injections of vehicle or TIMP2; 20-month-old). **g**, **h**, PSA recorded in dentate gyrus granule cell layer following perforant path stimulation in slices incubated with indicated *ex vivo* treatments (**g**) and maintenance-phase LTP quantification (**h**; $n = 10$ slices per group from $n = 7$, 4, 5 WT mice per group (left to right); 2-month-old mice). **i**, Discrimination for novel object displacement on day 2 for young WT mice treated every other day for 4 weeks with anti-TIMP2 IgG or control IgG ($n = 15$ per group; 2.5-month-old). **j–l**, Latency to escape hole in Barnes maze (**j**), day 4 acquisition rate (**k**), and contextual fear-conditioning freezing levels (**l**) in aged NSG mice (13.8 ± 0.1 months old) given eight intravenous injections of vehicle ($n = 10$), TIMP2-depleted cord plasma ($n = 8$), or IgG control-depleted cord plasma ($n = 9$) (in **j**, * and † indicate control-depleted cord plasma versus either vehicle or TIMP2-depleted cord plasma groups, respectively). One-way ANOVA with Tukey's post hoc test for **h**, **k**, **l**; two-way repeated-measures ANOVA with Bonferroni's post hoc test for **a**, **j**; Student's *t*-test for two-group comparisons; χ^2 analysis for **d**; two-way ANOVA with Tukey's post hoc test for **i**; $^*P < 0.05$, $^\#P = 0.05$, $^{**}P < 0.01$, †††† or $^{***}P < 0.001$, $^{****}P < 0.0001$; mean ± s.e.m.

treatment significantly improved the ability of aged WT mice to find the escape hole in the Barnes maze, while also enhancing acquisition rate (Fig. 4a, b). Contextual memory was significantly enhanced in aged mice after TIMP2 treatment (Fig. 4c), while baseline and cued freezing levels were unchanged (Extended Data Fig. 7s, t). Moreover, TIMP2 treatment significantly restored nesting ability (Fig. 4d), a behaviour strongly impaired in aged mice[26]. To examine whether TIMP2 altered plasticity on a synaptic level within the dentate gyrus, and in the absence of neurogenesis enhancements (Extended Data Fig. 8a, b), we again treated aged WT mice with TIMP2 and measured LTP from dentate gyrus synapses in slices. LTP was robustly increased in mice treated systemically with TIMP2 (Fig. 4e, f and Extended Data Fig. 8c), consistent with the learning and memory improvements observed. Conversely, LTP was significantly impaired in slices from TIMP2 KO mice compared with that measured from WT slices (Extended Data Fig. 8d, e). Young hippocampal slices incubated with anti-TIMP2 immunoglobulin-G (IgG) to target pools of brain TIMP2 exhibited markedly less LTP than control slices (Fig. 4g, h), arguing that locally acting TIMP2 is important for activity-dependent synaptic plasticity. Notably, this decrease in LTP was not observed after treatment of TIMP2 KO slices with control or anti-TIMP2 IgG (Extended Data Fig. 8f, g).

Given the age-related reduction of hippocampal TIMP2 expression and possible brain entry of TIMP2 after systemic treatment, we next assessed the necessity of blood-borne TIMP2 for hippocampal-dependent memory. We used novel location recognition, a spatial, hippocampal-dependent task that also avoids reliance on startle response behaviour (Extended Data Fig. 9a, b) and motor coordination perturbed with loss of TIMP2 function[27,28]. Young WT mice were given systemic injections of TIMP2 neutralization or control antibody for 4 weeks before novel location recognition testing. Antibody treatments did not alter overall metabolism, organ function, or weight gain (Extended Data Fig. 9c, d). Neither anxiety-linked open-field behaviour nor overall activity was altered by treatment (Extended Data Fig. 9e–i), which was verified in an independent activity task (Extended Data Fig. 9j–m). While neurogenesis was unaltered (Extended Data Fig. 9n, o), mice in which systemic TIMP2 had been targeted by TIMP2 antibody completely lost preference for the displaced object 1 day after training (Fig. 4i), suggesting a critical role of TIMP2 in spatial memory. Many immune and trophic factors were significantly upregulated in plasma from TIMP2 KO mice (Extended Data Fig. 10a), suggesting that TIMP2 may be a critical regulator in the systemic proteome and perhaps the systemic-CNS communicome.

To assess the necessity of TIMP2 in mediating cognitive improvements caused by cord plasma treatment, we first efficiently immunodepleted (>99%; Extended Data Fig. 10b) human TIMP2 from cord plasma without grossly depleting other proteins compared with control depletion (Extended Data Fig. 10c). After treatment of aged NSG mice with vehicle, control-depleted or TIMP2-depleted cord plasma, Barnes maze (Fig. 4j, k) and contextual fear-conditioning (Fig. 4l) assessments revealed a striking dependency on TIMP2 and its putative cofactors for the previously observed cognitive benefits conferred by cord plasma, especially in the Barnes maze. Other behavioural measures were unable to account for the cognitive differences among groups given the lack of differences in baseline and cued fear-conditioning freezing, open-field behaviour, and various activity measures (Extended Data Fig. 10d–m).

The necessity of TIMP2 for the beneficial activity of cord plasma and its ability to improve aspects of hippocampal function at an age when TIMP2 expression has declined suggest that it may be a critical mediator in mechanisms governing synaptic plasticity. Future studies should dissect the putative cellular targets of TIMP2 produced within the hilus and the extent to which these signals impinge on local circuitry to regulate activity of synapses throughout the hippocampus. Given the many potential targets in the brain, TIMP2 may exert its effects on plasticity through complex interactions with matrix metalloproteinases and integrins to regulate extracellular matrix and structural protein turnover[29]. Together, our results argue that systemic factors present early in life may be beneficial for revitalization of aged tissue and that TIMP2, a protein enriched during development[30], represents such a restorative factor for the aged hippocampus.

Online Content Methods, along with any additional Extended Data display items and Source Data, are available in the online version of the paper; references unique to these sections appear only in the online paper.

Received 19 November 2015; accepted 14 March 2017.
Published online 19 April 2017.

1. Burke, S. N. & Barnes, C. A. Neural plasticity in the ageing brain. *Nature Rev. Neurosci.* **7,** 30–40 (2006).
2. Cole, A. J., Saffen, D. W., Baraban, J. M. & Worley, P. F. Rapid increase of an immediate early gene messenger RNA in hippocampal neurons by synaptic NMDA receptor activation. *Nature* **340,** 474–476 (1989).
3. Dragunow, M. *et al.* Long-term potentiation and the induction of c-fos mRNA and proteins in the dentate gyrus of unanesthetized rats. *Neurosci. Lett.* **101,** 274–280 (1989).
4. Jones, M. W. *et al.* A requirement for the immediate early gene Zif268 in the expression of late LTP and long-term memories. *Nature Neurosci.* **4,** 289–296 (2001).
5. Verbitsky, M. *et al.* Altered hippocampal transcript profile accompanies an age-related spatial memory deficit in mice. *Learn. Mem.* **11,** 253–260 (2004).
6. Lund, P. K. *et al.* Transcriptional mechanisms of hippocampal aging. *Exp. Gerontol.* **39,** 1613–1622 (2004).
7. Lee, C. K., Weindruch, R. & Prolla, T. A. Gene-expression profile of the ageing brain in mice. *Nature Genet.* **25,** 294–297 (2000).
8. Blalock, E. M. *et al.* Gene microarrays in hippocampal aging: statistical profiling identifies novel processes correlated with cognitive impairment. *J. Neurosci.* **23,** 3807–3819 (2003).
9. Conboy, I. M. *et al.* Rejuvenation of aged progenitor cells by exposure to a young systemic environment. *Nature* **433,** 760–764 (2005).
10. Loffredo, F. S. *et al.* Growth differentiation factor 11 is a circulating factor that reverses age-related cardiac hypertrophy. *Cell* **153,** 828–839 (2013).
11. Sinha, M. *et al.* Restoring systemic GDF11 levels reverses age-related dysfunction in mouse skeletal muscle. *Science* **344,** 649–652 (2014).
12. Salpeter, S. J. *et al.* Systemic regulation of the age-related decline of pancreatic β-cell replication. *Diabetes* **62,** 2843–2848 (2013).
13. Baht, G. S. *et al.* Exposure to a youthful circulation rejuvenates bone repair through modulation of β-catenin. *Nature Commun.* **6,** 7131 (2015).
14. Katsimpardi, L. *et al.* Vascular and neurogenic rejuvenation of the aging mouse brain by young systemic factors. *Science* **344,** 630–634 (2014).
15. Villeda, S. A. *et al.* The ageing systemic milieu negatively regulates neurogenesis and cognitive function. *Nature* **477,** 90–94 (2011).
16. Villeda, S. A. *et al.* Young blood reverses age-related impairments in cognitive function and synaptic plasticity in mice. *Nature Med.* **20,** 659–663 (2014).
17. Castellano, J. M., Kirby, E. D. & Wyss-Coray, T. Blood-borne revitalization of the aged brain. *JAMA Neurol.* **72,** 1191–1194 (2015).
18. Shultz, L. D. *et al.* Human lymphoid and myeloid cell development in NOD/LtSz-scid IL2R gamma null mice engrafted with mobilized human hemopoietic stem cells. *J. Immunol.* **174,** 6477–6489 (2005).
19. Lee, Y. I., Park, K. H., Baik, S. H. & Cha, C. I. Attenuation of c-Fos basal expression in the cerebral cortex of aged rat. *Neuroreport* **9,** 2733–2736 (1998).
20. Faizi, M. *et al.* Thy1-hAPP$^{Lond/Swe+}$ mouse model of Alzheimer's disease displays broad behavioral deficits in sensorimotor, cognitive and social function. *Brain Behav.* **2,** 142–154 (2012).
21. Korb, E., Herre, M., Zucker-Scharff, I., Darnell, R. B. & Allis, C. D. BET protein Brd4 activates transcription in neurons and BET inhibitor Jq1 blocks memory in mice. *Nature Neurosci.* **18,** 1464–1473 (2015).
22. Malik, A. N. *et al.* Genome-wide identification and characterization of functional neuronal activity-dependent enhancers. *Nature Neurosci.* **17,** 1330–1339 (2014).
23. Guenthner, C. J., Miyamichi, K., Yang, H. H., Heller, H. C. & Luo, L. Permanent genetic access to transiently active neurons via TRAP: targeted recombination in active populations. *Neuron* **78,** 773–784 (2013).
24. Iwano, T., Masuda, A., Kiyonari, H., Enomoto, H. & Matsuzaki, F. Prox1 postmitotically defines dentate gyrus cells by specifying granule cell identity over CA3 pyramidal cell fate in the hippocampus. *Development* **139,** 3051–3062 (2012).
25. Boyd, T. D. *et al.* GM-CSF upregulated in rheumatoid arthritis reverses cognitive impairment and amyloidosis in Alzheimer mice. *J. Alzheimers Dis.* **21,** 507–518 (2010).
26. Cramer, P. E. *et al.* ApoE-directed therapeutics rapidly clear β-amyloid and reverse deficits in AD mouse models. *Science* **335,** 1503–1506 (2012).
27. Jaworski, D. M., Boone, J., Caterina, J., Soloway, P. & Falls, W. A. Prepulse inhibition and fear-potentiated startle are altered in tissue inhibitor of metalloproteinase-2 (TIMP-2) knockout mice. *Brain Res.* **1051,** 81–89 (2005).
28. Jaworski, D. M., Soloway, P., Caterina, J. & Falls, W. A. Tissue inhibitor of metalloproteinase-2(TIMP-2)-deficient mice display motor deficits. *J. Neurobiol.* **66,** 82–94 (2006).
29. Dityatev, A., Schachner, M. & Sonderegger, P. The dual role of the extracellular matrix in synaptic plasticity and homeostasis. *Nature Rev. Neurosci.* **11,** 735–746 (2010).
30. Blavier, L. & DeClerck, Y. A. Tissue inhibitor of metalloproteinases-2 is expressed in the interstitial matrix in adult mouse organs and during embryonic development. *Mol. Biol. Cell* **8,** 1513–1527 (1997).

Supplementary Information is available in the online version of the paper.

Acknowledgements We thank clinical staff for human blood-plasma collection/coordination, C. Guenthner, L. Luo for TRAP-FOS breeders, T. Rando for discussion, Stanford Translational Applications Service Center/Protein and Nucleic Acid facilities for whole-genome microarrays, H. Zhang for mice for depletion experiments. This work was funded by the Jane Coffin Childs Postdoctoral Fellowship-Simons Foundation (J.M.C), Veterans Affairs (T.W.-C.), anonymous (T.W.-C.), the Glenn Foundation for Medical Research (T.W.-C.), the Stanford Brain Rejuvenation Project, and the National Institute on Aging (K99AG051711 (J.M.C.), AG045034 (T.W.-C.), DP1AG053015 (T.W.-C.) and AG040877 (K.I.M.)).

Author Contributions J.M.C. and T.W.-C. designed research. J.M.C., K.I.M., D.B., and J.C.S. performed protein microarray experiments. J.M.C., R.J.A., and A.A.M. performed behaviour, staining/microscopy. J.M.C. performed biochemical assays; I.V.H. developed silver stain protocol. J.M.C. and M.L.J. performed radiolabelling/autoradiography experiments. J.M.C., B.Z., and X.S.X. performed LTP experiments. M.T. and M.S.A. provided human samples. J.M.C. analysed data and wrote the manuscript. T.W.-C. supervised study.

Author Information Reprints and permissions information is available at www.nature.com/reprints. The authors declare competing financial interests: details are available in the online version of the paper. Readers are welcome to comment on the online version of the paper. Publisher's note: Springer Nature remains neutral with regard to jurisdictional claims in published maps and institutional affiliations. Correspondence and requests for materials should be addressed to T.W.-C. (twc@stanford.edu).

Reviewer Information *Nature* thanks H. Eichenbaum and the other anonymous reviewer(s) for their contribution to the peer review of this work.

METHODS

Mice. Aged male WT C57BL/6 mice were obtained from the National Institute on Aging aged rodent colony. NOD.Cg-*Prkdcscid; Il2rgtm1Wjl*/SzJ mice[18] ('NSG' mice) on a NOD/ShiLtJ background, young TIMP2 knockout[28], or WT mice were obtained from Jackson Laboratories (unless otherwise indicated), bred, and maintained according to Jackson recommendations to minimize opportunistic infections. Persistent hyperactive behaviour in female NSG mice motivated the use of male mice in behavioural studies. All mice were kept on a 12-h light/dark cycle and provided *ad libitum* access to food and water. 'Vehicle' treatments consisted of phosphate-buffered saline (PBS) in all instances. All animal care and procedures complied with the Animal Welfare Act and were in accordance with institutional guidelines and approved by the V.A. Palo Alto Committee on Animal Research and the institutional administrative panel of laboratory animal care at Stanford University.

TRAP for c-Fos. Given the transient nature of c-Fos expression and the likelihood of adverse effects after chronic treatment of normal mice with human plasma, we used the TRAP-FOS (*FOS*$^{CreERT2/+}$; *R26*$^{AI14/+}$) mouse model[23] to examine c-Fos activation following neonatal plasma treatment. TRAP-FOS mice on a C57Bl/6J background were given a single intravenous injection of human plasma or vehicle (175 μl), followed 2 h later by intraperitoneal injection of the tamoxifen derivative 4-hydroxytamoxifen (4-OHT; 50 mg per kg; freshly prepared). Seventy-two hours after injection of 4-OHT, mice were euthanized for immunohistochemical analysis.

Parabiosis. Heterochronic parabiotic pairs consisting of aged and young mice (18-month-old with 3-month-old) or isochronic pairs consisting of aged mice (18-month-old with 18-month-old) were connected according to previously described methods[9,16,31]. Briefly, under aseptic conditions and continuous isoflurane anaesthesia, mirror-image incisions at left and right flanks were made through the skin with smaller incisions through the peritoneal cavity. Adjacent peritoneal cavities were sutured together continuously and closed. Knee and elbow joints from adjacent mice were sutured together to facilitate coordinated locomotion during recovery to minimize distress. Skin was stapled together using surgical autoclips (9-mm, Clay Adams). Surgeries were performed on heating pads and body temperature was monitored throughout the procedure. Mice in each pair were injected subcutaneously with Baytril antibiotic (5 μg per g) and buprenorphine (0.05–0.1 μg ml^{-1}) for pain management and 0.9% (w/v) NaCl for hydration. Pairs were monitored continuously for signs of distress according to recovery parameters characterized in previous work[31].

Human and mouse plasma collection and injections. Cord (live umbilical venous collection at birth), young, and elderly blood was collected for the isolation of ethylenediaminetetraacetate (EDTA)-plasma under Stanford Institutional Review Board consent and approval. Young (median = 22 years) and elderly (median = 66 years) healthy subjects were male and predominantly caucasian; elderly subjects were cognitively normal according to neurological examination. Isolated plasma was stored in aliquots at −80 °C until analysis or before pooling and dialysis to remove EDTA for treatment experiments where indicated. Intravenous injections of human plasma (175 μl) were administered six times for staining/qPCR experiments and eight times for behavioural and LTP experiments, with 2 days between each injection. Under 3.8% (w/v) chloral hydrate or 2.5% (v/v) avertin anaesthesia, mouse blood was collected with EDTA as anticoagulant by terminal intracardial bleeding. EDTA-plasma was isolated by centrifugation at 1,000*g* for 10 min at 4 °C before aliquoting and storage at −80 °C before analysis. In the anti-TIMP2 IgG- or control IgG-treated cohort of mice monitored for signs of toxicity, serum was collected at the conclusion of behavioural assessments. Under 2.5% avertin anaesthesia, blood was drawn by intracardial bleeding, allowed to clot for 45 min at room temperature, and then serum was collected by centrifugation at 2,000*g* for 10 min at 4 °C. Serum was submitted for measurement of electrolytes and other measures of organ function by the Animal Diagnostic Laboratory at Stanford Veterinary Service Center. One sample from each group was found to be haemolysed and thus not submitted to avoid confounding haemolysis-sensitive assays.

Plasma protein measurement. *Luminex-based detection, ELISA, western blotting.* Quantitative measurements for 66 detectable plasma biomarkers in Extended Data Fig. 1 were made by fee-for-service (Myriad RBM) using the multiplexed HumanMAP version 2.0 platform; two-way hierarchical clustering analysis was performed using Cluster 3.0 using correlation similarity metric distance. Left-censored values below detection were replaced with half the detection limit. Quantitative validation for candidate factors from customized protein microarray results identified from overlap analysis was done with commercially available ELISAs for CSF2 (human V-Plex, Meso Scale Diagnostics) and TIMP2 (human Quantikine, R&D Systems) according to the manufacturer's specifications. Equivalent volumes of plasma (2 μl) were loaded onto 4–12% bis-tris gels for SDS–polyacrylamide gel electrophoresis before transferring to nitrocellulose membranes for immunodetection of mouse TIMP2 (1:500; Rabbit mAb; Cell Signaling, D18B7). For hippocampal western blotting of TIMP2, dissected hippocampi were manually dounce-homogenized with 60 strokes in radioimmunoprecipitation assay buffer with protease inhibitors and briefly sonicated (5 s, three times, 15% amplitude; Branson Ultrasonics) before centrifugation at 20,000*g* for 25 min at 4 °C. Immunoblotting for TIMP2 was performed as described above, and neuron-specific enolase was immunoblotted for loading normalization (1:5,000; Mouse IgG; Thermo, 5E2). Band intensities were quantified using ImageJ software as described[32].

Protein microarrays. Customized mouse or human versions of protein microarrays were created, as described[33], solely as a discovery platform with which to identify promising hits that could be validated by subsequent, more quantitative assays. Specifically, ELISA-grade antibodies against several hundred secreted and potentially cleaved transmembrane mouse or human signalling proteins were obtained from commercial sources and printed in five replicates onto SuperEpoxy2 glass slides (Arrayit) with a robotic microarrayer (NanoPrint LM210, Arrayit) fitted with 16 946MP4B pins. Arrays were vacuum-sealed and stored at 4 °C until use. Before labelling with biotin, human or mouse plasma samples were diluted and dialysed (96-well Dispodialyzer, 5-kDa molecular weight cut-off, Harvard Apparatus), exchanging PBS (pH 6.5 for mouse and pH 8.0 for human arrays) multiple times at 4 °C. Samples were then biotinylated on primary amino groups (EZ-link NHS-Biotin, Thermo-Scientific) overnight at 4 °C, and unbound biotin was removed by PBS dialysis. Arrays were then blocked with 3% (w/v) casein solution before incubation with the individual biotinylated samples overnight at 4 °C. Following washes, arrays were incubated with Alexa Fluor 555-conjugated streptavidin secondary antibodies (Life Technologies) for detection of the fluorescent signals using a GenePix4400A scanner and GenePix Pro7 software (Molecular Devices). A complete list (HUGO Gene Nomenclature Committee official gene names) of all unique proteins we sought to detect with arrays for the generation of candidates is provided in Supplementary Table 1.

Protein microarray data processing and analysis. Background for fluorescent signals of individual array spots was subtracted and raw data average intensities were calculated from five replicates per antibody. Antibodies with insufficient signal to noise were filtered out. Negative values were imputed and replaced by 50% of the lowest values detected for a given antibody's signal. Log-transformation and iterative row- and column-wise median centering and normalization were performed using Cluster 3.0 (ref. 34) or log-transformed following a Shapiro–Wilk test to assess normality ($P < 0.05$). *Z*-scored values were used for unsupervised, array by protein cluster analysis before heat map visualization using Java TreeView 1.0.13 (ref. 35) on the basis of *d*-score rankings from SAM 3.0 algorithm[36]. Relative protein expression levels correlated with ageing or significantly different between aged isochronic and aged heterochronic plasma were determined by SAM. *d*-scores were assigned to each protein on the basis of multi-comparison analysis of expression changes across arrays. To generate a list of candidate proteins that might improve plasticity in aged mice, *d*-scores from SAM were used to rank proteins that declined with age in the mouse array, and a composite meta-ranking was made by comparing this to the *d*-scored proteins that declined in the human array (from cord to elderly). A list was created in the same way to capture cord-plasma-enriched proteins also elevated in the plasma of aged heterochronic mice (sharing young blood) versus aged-isochronic parabiont plasma. Extended Data Fig. 6a reflects sequential sorting by *q* value and *d*-score of the list. For limited *in vivo* screens, TIMP2, CSF2, and GAS6 were chosen from this list on the basis of literature review and availability of suitable recombinant protein. Pre- and post-surgery plasma from parabionts was also collected for comparison of changes, in addition to examining young and aged isochronic plasma protein changes for validation.

For subsequent mouse plasma experiments to examine relative protein abundance in TIMP2 KO versus WT mouse plasma (Extended Data Fig. 10a), mouse protein arrays were printed and run as described for earlier arrays; multiple steps of filtering of the raw data were performed on the basis of antibody performance before normalization during further optimization of the platform. Briefly, antibodies with low signal, large coefficient of variation across five replicate spots, or those with high coefficients of variation across four identical biological replicates (four random subjects run in four identical repeats) were filtered out. Non-detectable values were imputed and replaced by 50% of the lowest value detected for a given antibody. Each signal was normalized by the median of all signals on one array, followed by log-transformation after assessing normality (Shapiro–Wilk test, $P < 0.05$) and then *Z*-scoring across all arrays. After filtering, 123 antibodies were used for differential expression analysis. Student's *t*-test ($\alpha = 0.05$) was performed to compare differences between two groups with $q < 0.15$.

Extracellular electrophysiology. After eight systemic injections of the indicated human plasma versus vehicle (PBS) in either young or aged NSG mice or rTIMP2 (50 μg kg^{-1}) versus vehicle in aged WT mice, deep anaesthesia was induced with

isoflurane before mice were euthanized. Brains were removed and placed in ice-chilled artificial cerebrospinal fluid (in mM: NaCl 124.0, KCl 2.5, KH_2PO_4 1.2, $CaCl_2$ 2.4, $MgSO_4$ 1.3, $NaHCO_3$ 26.0 and glucose 10.0 (pH 7.4)) that was continuously bubbled with 5% CO_2/95% O_2. Hippocampal slices (400 μm) were prepared using a tissue chopper (Stoelting) and incubated in continuously oxygenated artificial cerebrospinal fluid for at least 1 h before recording with continuous 5% CO_2/95% O_2 bubbling. Data were collected using an Axopatch-2B amplifier and pClamp 10.4 software (Axon Instruments). Slices were in submerged mode at room temperature, continuously perfused with oxygenated artificial cerebrospinal fluid at a flow rate of 2 ml min^{-1} using a peristaltic pump (Haake Buchler). Population spikes were recorded in the granule cell layer of the dentate gyrus with glass microelectrodes (resistance 1–3 MΩ). Stimulation of the perforant path with biphasic current pulses (0.2 ms duration for one phase, 0.4 ms in total) was delivered in intervals of 10 s through a bipolar, concentric stimulating electrode (FHC). Using this frequency stimulation protocol, no obvious synaptic depression or facilitation was observed. Slices were recorded within 8 h of dissection. Signals were digitized at 20 kHz, and a Gaussian low-pass filter was applied as needed to reduce noise. Input–output curves were constructed for each slice using stimulus intensity from threshold to 1.0 mA. Test pulse intensities were adjusted to evoke field potential to approximately 35–50% of maximal input–output response. Tetanic stimulation was executed with two trains of 100 pulses (0.4 ms pulse duration, 100 Hz) delivered with an inter-train interval of 5 s. Amplitudes of population spikes were measured from the initial phase of the negative wave with Clampfit 10.4. LTP was plotted as the percentage of baseline just before tetanic stimulation (mean ± s.e.m.) and the graph scaled to reflect effects in the maintenance phase (first one or two points after baseline could be outside scale). The maintenance phase was quantified over the final 6 min (39.5–45.5 min) of the LTP experiment. Paired-pulse ratios were measured with various inter-pulse intervals (20 ms, 50 ms, 100 ms). Paired-pulse ratio was calculated before or after LTP as the percentage of the amplitude of the second response minus the first response divided by the value of the first response. In rare cases, values were not obtained at all time points owing to experimental or equipment error. Data were processed and analysed with pClamp 10.4, Microsoft Excel, and StatView 5.0.

For experiments in which isolated slices from young WT (C57Bl/6J) or TIMP2 KO mice were assessed, or for those in which slices were incubated with vehicle (PBS), control IgG (R&D) or anti-TIMP2 IgG (R&D, AF971), LTP was performed in essentially the same fashion but with minor differences. Briefly, tetanic stimulation consisted of one train of 100 pulses (0.4 ms pulse duration, 100 Hz) since preliminary experiments revealed that two trains of high-frequency stimulation in younger slices tended to create short-term depression of field potentials in dentate gyrus, lasting approximately 10 min. For experiments involving bath incubation of the isolated slices, we adapted a previously described method for antibody blocking experiments in the context of LTP[37,38]. Slices were incubated with fresh control IgG (R&D Systems) or anti-TIMP2 IgG (R&D Systems) at 4 μg ml^{-1} in a clean chamber for ~2 h (1.8 ± 0.2 h, IgG control; and 1.9 ± 0.3 h, anti-TIMP2 IgG) at room temperature before transferring to recording chamber. Antibodies or vehicle were perfused continuously through a closed loop during recording through silicon tubing (VWR) (with the exception of a 5-cm portion connected to the pump). BSA was omitted from perfusion to minimize bubbling; efforts were taken to minimize bubbling of artificial cerebrospinal fluid in the perfusion system that would perturb oxygen and pH consistency.

Recombinant protein injections. Recombinant mouse TIMP2 (R&D Systems) or CSF2 (Sino Biological) proteins were resuspended in physiological buffer, aliquoted and stored at −80 °C for single-injection use at 50 μg kg^{-1}. Mice were given systemic injections (intraperitoneal) of vehicle or recombinant protein every other day at frequency and durations indicated in the respective figure legends.

Plasma TIMP2 immunodepletion. To remove TIMP2 present in human umbilical cord plasma, anti-TIMP2 IgG (R&D) or goat control IgG (R&D) were efficiently conjugated to 2.8-μm superparamagnetic M-270 Epoxy dynabeads according to the manufacturer's instructions (ThermoFisher) using a coupling ratio of 5 μg of antibody per 1 mg of beads for 24-h covalent conjugation at 37 °C with end-over-end rotation. Steps were taken to minimize detergent carryover in certain steps, for example substitution with PBS, in preparation for treatments *in vivo*. Freshly dialysed cord plasma from the collections of nine individuals was thawed, pooled, and divided into 500-μl aliquots before incubation with prepared control IgG-bead or anti-TIMP2 IgG-bead solutions overnight at 4 °C. An aliquot of cord plasma without beads was carried through the procedure to verify no loss due to handling/degradation. Isolated control IgG-depleted or anti-TIMP2 IgG-depleted plasma was frozen and stored in preparation for injections of aged NSG mice. Human TIMP2 ELISA on the pooled, depleted plasma revealed TIMP2 levels well below the detection limit of the assay compared with levels measured in cord plasma aliquot before depletion ('pre-depletion'), and no reduction was detected in control IgG-depleted plasma (Extended Data Fig. 10b). Complete elution of the beads in denaturing/reducing conditions was performed, and the resulting elution was separated by SDS–polyacrylamide gel electrophoresis before silver staining according to standard methods. Briefly, gel was incubated in 10% acetic acid/50% methanol (fixation), sensitized in 2.5 mM sodium thiosulfate, silver stained in silver nitrate (12 mM), and developed in a solution of sodium carbonate (0.3 M), sodium thiosulfate (25 μM), and formaldehyde (0.02% (w/w)). The silver-stained gel revealed a depletion pattern that was indistinguishable between the IgG control or anti-TIMP2 IgG depletion conditions (Extended Data Fig. 10c).

Mouse behavioural assays. A modified Barnes maze test was performed similarly to that previously described[20], and tailored minimally to our strains of mice. Briefly, a large circular maze containing 40 holes was centred over a pedestal and elevated approximately 40 cm above the floor. The escape hole consisted of a long PVC elbow joint connector that was similar in texture and colour to the maze. Distinct visual cues were placed at four equally spaced points around the maze, as shown in Extended Data Fig. 2g. An overhead light provided additional motivation to find the escape hole. The task proceeded over a period of 4 days, with four trials on each day for each mouse. With overhead illumination and a persistent 2 kHz tone, mice were given 90 s for each trial to identify the escape hole by jumping in or identifying the hole with extended/overt head pokes. If mice failed to identify the escape hole within the allotted 90 s, they were gently guided by light tapping/directing towards the escape hole and scored at the allotted investigation time. The escape hole position was fixed within a day but changed for each successive day of testing. For each trial within a day, the starting location for the mouse was rotated relative to the escape hole position. Between each trial, the maze and escape hole were thoroughly cleaned to remove any cues that might affect performance in subsequent trials.

Several sensory modalities were assessed in young and aged NSG mice. Pain sensitivity to the foot-shock apparatus used for fear-conditioning was assessed using the procedure described in ref. 39. In this assay, each mouse was placed in the foot-shock chamber with a front-mounted camera to visualize various pain sensitivity parameters, which encompassed four clearly defined behaviours, as described[39,40]: 'flinch', 'run', 'vocalization', and 'two-paw jump'. One-second shocks of various intensities were delivered in the following order (in milliamps): 0.05, 0.08, 0.10, 0.13, 0.16, 0.20, 0.25, 0.30, 0.35, 0.40, 0.45, each spaced by 30 s of recovery time. Thresholds reflected the minimum shock intensity at which each behaviour was observed using the front-mounted camera video. To assess visual ability, the visual cliff task was adapted according to the classical method[41], a task recently used to detect complex age-related visual deficits in models of neurodegeneration[42] as a means of validating spatially dependent cognitive assays. Briefly, a chamber was constructed with dimensions 60 cm × 60 cm × 30 cm using white plastic and a transparent (non-glare) bottom. The fabricated box was extended halfway across a table elevated 1 m above the floor. Chequered fabric served as the floor below the box, which then draped downwards, extending onto the floor to create the visual cliff illusion. A series of light sources illuminated the chamber interior to prevent dark retreat areas, and an additional light was directed towards the edge to accentuate the cliff illusion. Two trials were performed for each mouse; a stopwatch was used to score the time elapsed before stepping onto the 'cliff side' as well as the duration spent on the 'bench side' or 'cliff side' of the chamber in the 5-min period. The auditory startle response assay was used to assess auditory sensory processing (Kinder Scientific). Each mouse was placed in a non-restrictive, ventilated, sound-attenuated chamber atop a sensor platform. After a 5-min acclimation period inside the chamber, startle sensitivity to various audible pulses (80, 90, 100, 110, 120 dB) was recorded. Five trials of each sound intensity were performed for each mouse, and each trial was presented once in a random sequence within each test session block with a variable inter-trial interval of 12–30 s (15 s on average). Startle response amplitudes were recorded and analysed via software interface (StartleMonitor), and the maximum response to each sound stimulus across the five trials was considered the acoustic response. All trials were performed in the same apparatus to minimize system error across trials, and aged and young mice were tested in a randomized sequence. The apparatus was calibrated using a standard 100-g weight.

For enriched housing exploration experiments to examine c-Fos activation under conditions of physiological neuronal activity, aged WT mice were treated systemically with vehicle or rTIMP2 (50 μg kg^{-1}) over a period of 1 week before a 10-min exposure to enriched housing (toy ball, tunnel, toy car, bell, blocks, wall-mounted visual cues, etc.). After the exploration, mice in enriched housing were returned to home cages for 90 min before being euthanized.

In young WT mice that had been injected with 60 μg kg^{-1} anti-TIMP2 antibody (R&D Systems, AF971; dose based on the *in vitro* ND_{50} (50% neutralizing dose from the manufacturer) or goat control IgG (R&D Systems), novel location recognition was performed as previously described[43]. Briefly, on day 1 (training),

mice were first habituated to the open-field arena, which contained wall-mounted visual cues, for a period of 6 minutes. Mice were given three consecutive trials during which they explored two objects in fixed positions. On day 2, mice explored the same arena but with one object displaced. Investigative interactions with objects were manually scored in a blinded fashion to assess object discrimination: that is, percentage object discrimination = ((displaced object interaction time)/(total interaction time of both objects)) × 100.

To assess anxiety-like and general exploratory activity levels, an open-field assay was used in which mice were placed in an illuminated, novel arena for 360 s and allowed to explore. Open-field exploratory behaviour was analysed using TopScan Lite software (Cleversys), which divided the chamber into a centre zone, in which mice tended to exhibit anxiety-associated activity, and the floor zone, in which mice exhibited normal activity behaviour. The SMARTCage beam-break monitoring system was used to assess general measures of activity in a home-cage-sized arena[31], which allowed activity assessment independent of anxiety-like behaviours associated with open-field exploration. Briefly, mice were placed inside monitored home cages that were each lined with bedding and covered with a cage top. Measures of activity (overall activity, rearing activity, distance travelled, average velocity) were recorded and analysed using the CageCenter tracking software/computer interface over the 360-s period of exploration.

Fear-conditioning experiments were performed as previously described[15,16]. Briefly, mice were trained to associate the cage context with an aversive stimulus (light foot-shock), allowing us to measure freezing levels indicative of hippocampal-dependent memory. Our protocol for NSG (NOD/ShiLtJ background) and WT (C57Bl/6 background) mice differed slightly. For NSG mice, training parameters on day 1 were as follows: two periods of 30 s consisting of paired cue light and 1,000-Hz tone followed by 2 s foot-shock (0.7 mA) with a 180-s interval between. On day 2 of testing, NSG mice exhibited recall after 90 s in context and freezing levels were analysed for the subsequent 90 s. The cued task was performed by changing the cage context (fabricated inserts with novel texture, colour, and odorant). Mice were placed in the novel context and exposed to the same tone and cue light from day 1 (training) after 180 s of exploration. Freezing levels were analysed for the subsequent 90 s. Fear-conditioning training for WT mice on a C57Bl/6 background used the following parameters: two periods of 30 s consisting of paired cue light and 1,000-Hz tone followed by a 2-s foot-shock (0.6 mA) with a 180-s interval between. The following day, mice were re-exposed to the context where freezing levels (recall) were particularly striking for the last 120 s for TIMP2 treatment or the first 120 s with CSF2 treatment. For the cued task, mice were placed in a novel context and exposed to the same tone and cue light from day 1 (training) after 120 s of exploration. Freezing levels were analysed for the subsequent 90 s. All freezing levels were measured using a FreezeScan video tracking system (Cleversys). Owing to variation in baseline cognitive performance reported previously for aged WT (C57Bl/6 background) mice[43] and routinely observed in our experience, aged WT mice were exposed to novel location recognition testing, as previously described[43], to score hippocampal-dependent memory performance. These values were used to divide mice equally into the two groups well before treatments and subsequent behavioural testing. After treatment of the equally stratified groups, blinded identification numbers were assigned to all mice, and the numbers were randomized for Barnes maze and fear-conditioning tests.

Immunohistochemistry. Brain tissue processing, immunohistochemistry, and immunofluorescence experiments were performed as described previously[15,16]. Briefly, mice were euthanized with 3.8% (w/v) chloral hydrate or 2.5% (v/v) Avertin and transcardially perfused with chilled 0.9% (w/v) saline or PBS. Brains were dissected and hemibrains were isolated for immunohistochemistry and post-fixed in 4% (w/v) paraformaldehyde for 48 h at 4 °C before preservation in 30% (w/v) sucrose in PBS. Hemibrains were sectioned coronally at a thickness of 40 μm on a freezing–sliding microtome, and sections were stored in cryoprotective medium at −20 °C. Free-floating sections were blocked with appropriate serum before incubation at 4 °C with primary antibodies at the following concentrations for light microscopy: c-Fos, 1:10,000, PC38, Oncogene Research Products; doublecortin (DCX), 1:500, SC8066, Santa Cruz Biotech; CD68, 1:600, MCA1957, BioRad; pCREB, 06-519, 1:5,000, Millipore; and the following concentrations for confocal microscopy: c-Fos, 1:400, 9F6, Cell Signaling; Gad67, 1:2,000, MAB5406, Millipore; Prox1, 1:500, AF2727, R&D Systems; NeuN, 1:200, MAB377, Millipore; mCherry, 1:200, AB0040-200, Sicgen; TIMP2, 1:100 (two nights), AF971, R&D Systems; Iba1, 1:500, 019-19741, Wako; and TO-PRO-3, 1:1,000, T3605, Life Technologies. For light microscopy, staining was visualized by incubating sections with respective biotinylated secondary antibodies, followed by reaction with the ABC kit (Vector) and diaminobenzidine (DAB; Sigma) staining. Images of brain sections were acquired by automated slide scanner (Hamamatsu Photonics) or by conventional light microscopy. National Institutes of Health ImageJ software was used to quantify the percentage of hippocampal area covered by thresholded CD68 staining or mean intensity for pCREB. The number of DCX-positive cells within the dentate gyri was counted manually and the total estimated as described[15] for both hemispheres. The number of c-Fos-positive cells in dentate gyrus was determined in five regularly spaced sections from the rostral to caudal extent of the hippocampus and doubled to account for both hemispheres. Manual counts of the number of c-Fos-positive cells present in three regularly spaced sections of lateral/basolateral amygdala and retrosplenial/motor cortex were made starting at −1.38 mm with respect to bregma in the mouse Scalable Brain Atlas[44,45]. All counts were performed in a blinded fashion.

For immunofluorescence experiments, after incubation with fluorescently conjugated secondary antibodies, brain sections were mounted and coverslipped with ProLong Gold (Life Technologies) before imaging with a confocal laser-scanning microscope (Zeiss). Absolute counts of the number of c-Fos-positive cells (or FOS-TRAPed cells) or co-stained cells were obtained through the entire z plane (~40 μm) using five sections per mouse for hippocampus (rostral through caudal extent of dentate gyrus) or the procedure described above for lateral/basolateral amygdala and retrosplenial/motor cortex counts. Co-localization was assessed at 1 Airy unit for each laser. Tile-scanning was performed for representative images taken for TRAP-FOS mice to provide high-resolution images of large areas of CA1 and dentate gyrus. Four sections per mouse (rostral through caudal extent of dentate gyrus) were used to count $TIMP2^+$ cells possessing $NeuN^+$ or $NeuN^-$ nuclei or $TIMP2^+$ cells co-expressing Iba1 within the dentate gyrus (subgranular zone and hilar subregions) of the hippocampus through a 25.6-μm z-stack acquired using a pinhole of 1 Airy unit for each laser. Optimization experiments revealed that TIMP2 KO sections were devoid of signal, validating the specificity of the TIMP2 antibody (Extended Data Fig. 7e). $TIMP2^+$ cells in dentate gyrus/hilus were consistent with the localization pattern observed in bacterial artificial chromosome (BAC)-TIMP2–eGFP (enhanced green fluorescent protein) mice as part of the GENSAT Project's mouse brain expression atlas (http://www.gensat.org/imagenavigator.jsp?imageID=72836).

Radiolabelled TIMP2 blood-to-brain tracer studies. *DOTA conjugation*. Conjugation of recombinant mouse TIMP2 (R&D) and BSA (Sigma) with 1,4,7,10-tetraazacyclododecane-1,4,7,10-tetraacetic acid (DOTA) was performed according to standard published procedures using metal-free buffers[46,47]. Briefly, a solution of DOTA-NHS ester (Macrocyclics) in dimethyl sulfoxide (25 mmol l^{-1}; 9–12 μl) was added to 200 μl of HEPES buffer (0.1 mol l^{-1}, pH 8.8) containing 100 μg of TIMP2 or BSA, and the reaction mixture was incubated at room temperature for 1 h. Excess DOTA-NHS was removed by Zeba Spin Desalting Columns (0.5 ml, 7K molecular weight cut-off, ThermoFisher Scientific), and the resulting solution was buffer-exchanged into ammonium acetate buffer (0.1 M, pH 5.5) for ^{64}Cu labelling. DOTA-conjugate solutions were concentrated by ultrafiltration (Vivaspin 0.5 ml, Sartorius) to 0.1–0.4 mg ml^{-1} and stored at 4 °C before radiolabelling. For TIMP2, all conjugation steps were performed <6 h before radiolabelling, and the final DOTA-conjugated protein was kept on ice. The numbers of chelators coupled per TIMP2 or BSA were estimated to be 2 and 2.2 respectively, by matrix-assisted laser desorption/ionization time-of-flight mass spectrometry.

Radiolabelling. Radiolabelling of DOTA–TIMP2 and DOTA–BSA with ^{64}Cu (half-life = 12.7 h) was performed using standard methods with some modifications[46–48]. In brief, DOTA–TIMP2 (25 μg) or DOTA–BSA (25 μg) in 50 μl of 0.25 mol l^{-1} ammonium acetate buffer (0.1 M, pH 5.5) was mixed with pH-balanced $[^{64}Cu]Cl_2$ solution (44–74 MBq, pH 5–5.5, University of Wisconsin, Madison) at 37 °C with gentle shaking at 300 r.p.m. After incubation (30 min for TIMP–DOTA and 60 min for BSA–DOTA), 0.1 M EDTA (0.5 M, pH 8.0) was added to a final concentration of 0.01 M and incubated at room temperature for 15 min to scavenge unchelated $[^{64}Cu]Cl_2$ in the reaction mixture. Purification of ^{64}Cu-labelled DOTA–TIMP2 and ^{64}Cu-labelled DOTA–BSA was achieved by G25 Sephadex size-exclusion purification (PD-10 column). Radiochemical purity was determined by instant thin-layer chromatography with TEC-Control Chromatography strips (Biodex Medical Systems, Shirley, New York), developed in saline, and size-exclusion liquid chromatography with a Phenomenex SEC 3000 column (Torrance, California, USA) with sodium phosphate buffer (0.1 mol l^{-1}, pH 6.8) at a flow rate of 1.0 ml min^{-1}. ^{64}Cu-labelled DOTA–TIMP2 and ^{64}Cu-labelled DOTA–BSA were obtained with high specific radioactivity (>75 GBq μmol^{-1}), radiochemical purity (>99%), and labelling efficiency (66–73%), and formulated in PBS (0.1 mol l^{-1} NaCl, 0.05 mol l^{-1} sodium phosphate (pH 7.4)).

Injections of radiolabelled TIMP2 in animals. Mice were given single intraperitoneal injections of either ^{64}Cu-labelled DOTA–TIMP2 (1.59 ± 0.09 MBq) or ^{64}Cu-labelled DOTA–BSA (2.50 ± 0.06 MBq). After 1, 3, or 24 h, groups of mice injected with each tracer were deeply anaesthetized with 2.5% (v/v) Avertin, and blood samples (100–200 μl) were collected by cardiac puncture immediately before transcardial perfusion with ~30 ml chilled PBS. The brain was extracted from each mouse, placed in a tube for gamma counting, and weighed; satisfactory perfusions

were verified by visual inspection of brain tissue. Tissue-associated radioactivity in blood and brain was assessed by an automated gamma counter (Cobra II Auto-Gamma counter; Packard Biosciences), normalized to tissue mass and to amount of radioactivity administered to each mouse, and decay-corrected to time of tracer injection using diluted aliquots of the initial administered dose as standards.

Ex vivo *autoradiography*. At 24 h after injection of ^{64}Cu-labelled TIMP2 (7.57 ± 0.15 MBq), mice were deeply anaesthetized with 2.5% (v/v) Avertin and perfused with ~30 ml chilled PBS. Brain tissue was quickly embedded in optimal-cutting temperature compound (Tissue-Tek), and coronal or sagittal sections (20 μm) were obtained for *ex vivo* autoradiography. Autoradiography was conducted using previously described methods[49], confirming anatomical localization by Nissl staining (cresyl violet acetate; Sigma Aldrich) using standard techniques. In brief, sections of 20 μm were mounted on microscope slides (Fisherbrand Superfrost Plus Microscope Slides), air-dried for 10 min, and then exposed to a digital storage phosphor screen (Perkin Elmer, USA) for 72 h at −20 °C. The image plate was analysed using a Typhoon 9410 Variable Mode Imager (Amersham Biosciences, USA) and images were visualized and processed by ImageJ (image processing and analysis software in Java, version 1.45s).

Metabolic stability studies. Stability of ^{64}Cu-labelled TIMP2 in mouse brain 24 h after intraperitoneal injection of radiotracer (19.27 ± 1.32 MBq) was determined as described previously[50] with minor modifications, including the use of a Bioscan Flow-Count radioactivity detector to enable sensitive detection of potential radiometabolites. Briefly, mice were deeply anaesthetized with 2.5% (v/v) Avertin, and perfused with chilled PBS (~30 ml) 24 h after intraperitoneal injection of ^{64}Cu-labelled TIMP2. Brain tissue was quickly collected and transferred to a tube containing 750 μl ice-cold 70:30 methanol:sodium phosphate buffer (0.1 M, pH 6.8). Samples were homogenized using an Omni TH tissue homogenizer, and protein precipitates were sedimented by centrifugation (9,400*g*, 10 min). Each supernatant (100 μl) was analysed via high-performance liquid chromatography (fitted with a highly sensitive positron detector for radioactivity) using size-exclusion liquid chromatography with a Phenomenex SEC 3000 column (Torrance, California, USA) and sodium phosphate buffer (0.1 mol l^{-1}, pH 6.8) at a flow rate of 1.0 ml min^{-1}. The percentage ratio of intact ^{64}Cu-labelled TIMP2 ($t_R = 11.5$ min) was calculated as (peak area for ^{64}Cu-labelled TIMP2/total area of all peaks) × 100. More than 95% of the radioactivity was recovered from the column for the analysed samples.

qPCR and whole-genome microarrays. After rapid dissection of hippocampi, tissue was preserved in RNA-later (Ambion) at 4 °C before storing at −80 °C until use. Hippocampal RNA was extracted according to the manufacturer's instructions using an RNeasy Mini Kit (Qiagen). Bioanalyzer (Agilent Technologies) quality control revealed high-quality RNA as assessed by RNA integrity number. Isolated RNA was used for transcription, labelling, and hybridization to whole-genome microarrays (Affymetrix, Mouse 2.0ST; with the assistance of Stanford Translational Applications Service Center/Protein and Nucleic Acid facilities) or to prepare cDNA with the RT^2 First Strand kit (SABiosciences) for qPCR. Samples were mixed with the RT^2 SYBR Green master mix (HotStart DNA *Taq* Polymerase, SABiosciences) and validated primers for key synaptic plasticity transcripts (RT^2 Profiler Kit, SABiosciences), before loading as technical duplicates for qPCR on a LightCycler 480 (Roche). C_T values for tissue were normalized to four common reference genes as recommended by manufacturer. The $\Delta\Delta C_T$ method was used to provide gene expression values[51]. For whole-genome microarrays, gene expression for annotated genes was normalized and analysed using R package 3.1.2/Bioconductor, and two-way hierarchical clustering was performed using a correlation similarity metric distance. Whole-genome microarray data can be obtained using accession numbers E-MTAB-4087 or GSE75416 at ArrayExpress or GEO, respectively. Gene Ontology-based activation analysis was performed on significantly changed annotated genes with Ingenuity Pathway Analysis suite's (Qiagen) Comparison Analysis tool to compare predicted pathway activation states across treatments using networks of changed genes and literature-based functional information. The software integrates gene changes with functional annotation information to predict an activation related to the degree and direction of gene changes in that category.

Statistics. Two-group comparisons were made using two-tailed, unpaired Student's *t*-test. For comparisons of more than two groups, one-way ANOVA followed by Tukey's post-hoc test was used. For comparisons of multiple factors (for example, time × treatment), two-way ANOVA was used before post-hoc testing. Repeated-measures two-way ANOVA with Bonferroni's post-hoc test was used for trial/day × treatment comparisons with repeated observations. Numbers of mice were estimated to be sufficient to detect statistically meaningful differences of at least 20% between or among groups using standard power calculations with $\alpha = 0.05$ and power of 0.8 on the basis of pilot or similar experiments. Homogeneity of variance was assessed, and appropriate corrections were made if necessary. All experiments were performed in a randomized and blinded fashion. Data were analysed statistically using GraphPad Prism 6.0, the R 3.1.2 package for Extended Data Fig. 1 and Fig. 1b, c, and SAM 3.0 for protein microarrays. The value of α was 0.05, and data are expressed as mean ± s.e.m. $^*P < 0.05$; $^{**}P < 0.01$; $^{***}P < 0.001$; $^{****}P < 0.0001$.

Data availability. Source Data are provided or are available from the corresponding author upon reasonable request.

31. Castellano, J. M. *et al. In vivo* assessment of behavioral recovery and circulatory exchange in the peritoneal parabiosis model. *Sci. Rep.* **6,** 29015 (2016).
32. Castellano, J. M. *et al.* Human apoE isoforms differentially regulate brain amyloid-β peptide clearance. *Sci. Transl. Med.* **3,** 89ra57 (2011).
33. Jaeger, P. A., Villeda, S. A., Berdnik, D., Britschgi, M. & Wyss-Coray, T. in *The Omics: Applications in Neuroscience* (ed Coppola, G.) 183–191 (Oxford Univ. Press, 2014).
34. de Hoon, M. J., Imoto, S., Nolan, J. & Miyano, S. Open source clustering software. *Bioinformatics* **20,** 1453–1454 (2004).
35. Saldanha, A. J. Java Treeview—extensible visualization of microarray data. *Bioinformatics* **20,** 3246–3248 (2004).
36. Tusher, V. G., Tibshirani, R. & Chu, G. Significance analysis of microarrays applied to the ionizing radiation response. *Proc. Natl Acad. Sci. USA* **98,** 5116–5121 (2001).
37. Chen, G., Kolbeck, R., Barde, Y. A., Bonhoeffer, T. & Kossel, A. Relative contribution of endogenous neurotrophins in hippocampal long-term potentiation. *J. Neurosci.* **19,** 7983–7990 (1999).
38. Kang, H., Jia, L. Z., Suh, K. Y., Tang, L. & Schuman, E. M. Determinants of BDNF-induced hippocampal synaptic plasticity: role of the Trk B receptor and the kinetics of neurotrophin delivery. *Learn. Mem.* **3,** 188–196 (1996).
39. Podhorna, J., McCabe, S. & Brown, R. E. Male and female C57BL/6 mice respond differently to diazepam challenge in avoidance learning tasks. *Pharmacol. Biochem. Behav.* **72,** 13–21 (2002).
40. Schrott, L. M. & Crnic, L. S. Sensitivity to foot shock in autoimmune NZB × NZW F1 hybrid mice. *Physiol. Behav.* **56,** 849–853 (1994).
41. Frank, R. & Kenton, J. Visual cliff behavior of mice as a function of genetic differences in eye characteristics. *Psychon. Sci.* **4,** 35–36 (1966).
42. Lione, L. A. *et al.* Selective discrimination learning impairments in mice expressing the human Huntington's disease mutation. *J. Neurosci.* **19,** 10428–10437 (1999).
43. Baruch, K. *et al.* Aging-induced type I interferon response at the choroid plexus negatively affects brain function. *Science* **346,** 89–93 (2014).
44. Bakker, R., Tiesinga, P. & Kötter, R. The Scalable Brain Atlas: instant Web-based access to public brain atlases and related content. *Neuroinformatics* **13,** 353–366 (2015).
45. Lein, E. S. *et al.* Genome-wide atlas of gene expression in the adult mouse brain. *Nature* **445,** 168–176 (2007).
46. Ilovich, O. *et al.* Development and validation of an immuno-PET tracer as a companion diagnostic agent for antibody-drug conjugate therapy to target the CA6 epitope. *Radiology* **276,** 191–198 (2015).
47. Cooper, M. S. *et al.* Comparison of ^{64}Cu-complexing bifunctional chelators for radioimmunoconjugation: labeling efficiency, specific activity, and in vitro/in vivo stability. *Bioconjug. Chem.* **23,** 1029–1039 (2012).
48. Zeng, D. *et al.* Microfluidic radiolabeling of biomolecules with PET radiometals. *Nucl. Med. Biol.* **40,** 42–51 (2013).
49. James, M. L. *et al.* New positron emission tomography (PET) radioligand for imaging σ-1 receptors in living subjects. *J. Med. Chem.* **55,** 8272–8282 (2012).
50. Boswell, C. A. *et al.* Comparative in vivo stability of copper-64-labeled cross-bridged and conventional tetraazamacrocyclic complexes. *J. Med. Chem.* **47,** 1465–1474 (2004).
51. Livak, K. J. & Schmittgen, T. D. Analysis of relative gene expression data using real-time quantitative PCR and the $2^{-\Delta\Delta C_T}$ method. *Methods* **25,** 402–408 (2001).

a

Donor Group	*N*	Mean age ± sd (yrs)	Mean gestational age ± sd (wks)	% Male	% Caucasian	Mean APGAR	Mean MMSE ± sd
Cord	7	NA	39 ± 0.58	100	100	9	NA
Young	12	21.11 ± 1.47	NA	100	100	NA	NA
Elderly	11	67.93 ± 6.39	NA	100	100	NA	29.6 ± 0.8

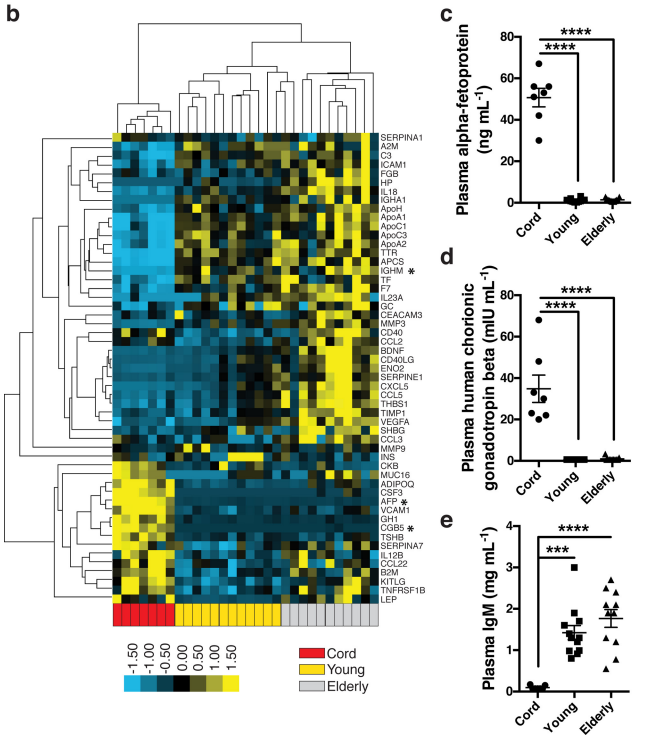

Extended Data Figure 1 | Expression of common plasma proteins differs according to donor group. a, Basic demographic characteristics of human subjects providing EDTA-plasma for corresponding quantitative analysis in **b**, and used for injections in Fig. 1. For umbilical cord plasma samples from neonates, gestational age reflects full-term births, and the APGAR is a composite health score reflecting appearance, pulse, grimace, activity, and respiration 5 min after birth. Mini-mental state examination (MMSE) is a 30-point neurological assessment of cognitive impairment (0-30, where 30 is least impairment). **b**, Heat map from unsupervised hierarchical cluster analysis of multiplexed plasma protein markers for cord, young adult, or elderly subjects (blue and yellow shades represent lower and higher relative expression, respectively; asterisks denote factors for which scatter plots are shown in **c**–**e**). **c**–**e**, Multiplex quantification of plasma α-fetoprotein (AFP), human chorionic gonadotropin (CGB5), and immunoglobulin-M (IgM) demonstrating significant donor-dependent differences. One-way ANOVA followed Tukey's post hoc test; $^{****}P < 0.0001$, $^{***}P < 0.001$; $n = 7$ (cord), $n = 12$ (young), $n = 11$ (elderly); mean ± s.e.m.

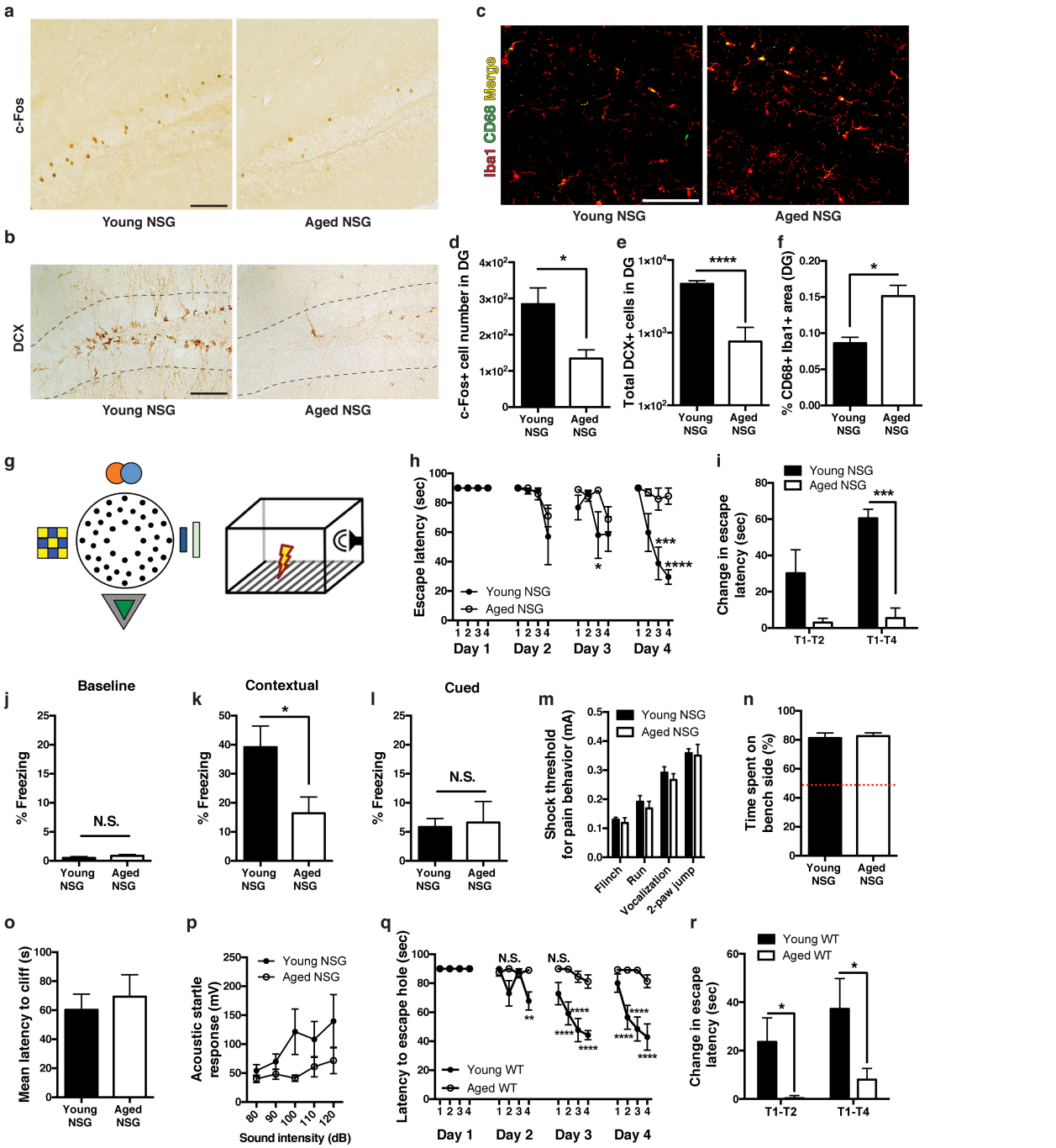

Extended Data Figure 2 | Immunodeficient NSG mice exhibit age-dependent hippocampal dysfunction independent of sensory function. **a**–**c**, Representative images of young and aged NSG hippocampi stained for c-Fos (**a**; $n = 7$ mice per group; male; 4.1 ± 0.2 versus 11.1 ± 0.1 months old), newborn neuron marker doublecortin (**b**; DCX) (female mice at 4.1 ± 0.1 months old ($n = 8$) and 10.9 ± 0.1 months old ($n = 7$)), and microgliosis (**c**), as indicated by confocal microscopy (yellow) of $Iba1^{+}CD68^{+}$ staining (female mice at 4.1 ± 0.1 months old ($n = 8$) and 10.9 ± 0.1 months old ($n = 7$); for **a**–**c**, scale bars are 100 μm). **d**–**f**, Quantification of indicated areas in **a**–**c**. **g**, Schematic diagram of modified Barnes maze (left) and contextual fear-conditioning tasks (right). **h**, Four-day trial time course for modified Barnes maze showing escape hole latency for young and aged NSG mice ($n = 4$ per group; 4.5-month-old versus 11.2-month-old). **i**, Change in escape latency (acquisition rate) between indicated trials on day 4 of Barnes maze testing. **j**–**l**, Freezing levels for young and aged NSG mice at baseline (**j**), during exposure to previously aversive fear-conditioning context (**k**), or during exposure to chamber with training cues but new context (**l**) ($n = 8$ mice per group; 3.1 ± 0.1 versus 12.1 ± 0.1 months old). **m**, Thresholds for various pain-related behaviours using foot-shock grid ($n = 6$ NSG mice per group; 4.1 ± 0.1 versus 12.3 ± 0.3 months old). **n**, **o**, Proportion of time spent on bench (safe) side (**n**) and mean latency before stepping over cliff side (**o**) during the visual cliff task to assess visual ability ($n = 10$ NSG mice per group; 3.6 ± 0.2 versus 13.3 ± 0.1 months old). **p**, Acoustic startle response at various sound intensities ($n = 10$ mice per group; 3.6 ± 0.2 versus 13.3 ± 0.1 months old). **q**, Four-day trial Barnes maze time course showing latency to target hole for young ($n = 9$) and aged ($n = 10$) WT (C57Bl/6) mice (3-month-old versus 21-month-old). **r**, Change in escape latency (acquisition rate) between indicated trials on day 4 of Barnes maze testing. Two-way repeated-measures ANOVA with Bonferroni's post hoc test for time × group comparisons; two-way ANOVA for stimulus × group comparisons; Student's *t*-test for two-group comparisons. $^{*}P < 0.05$, $^{***}P < 0.001$, $^{****}P < 0.0001$; mean ± s.e.m.

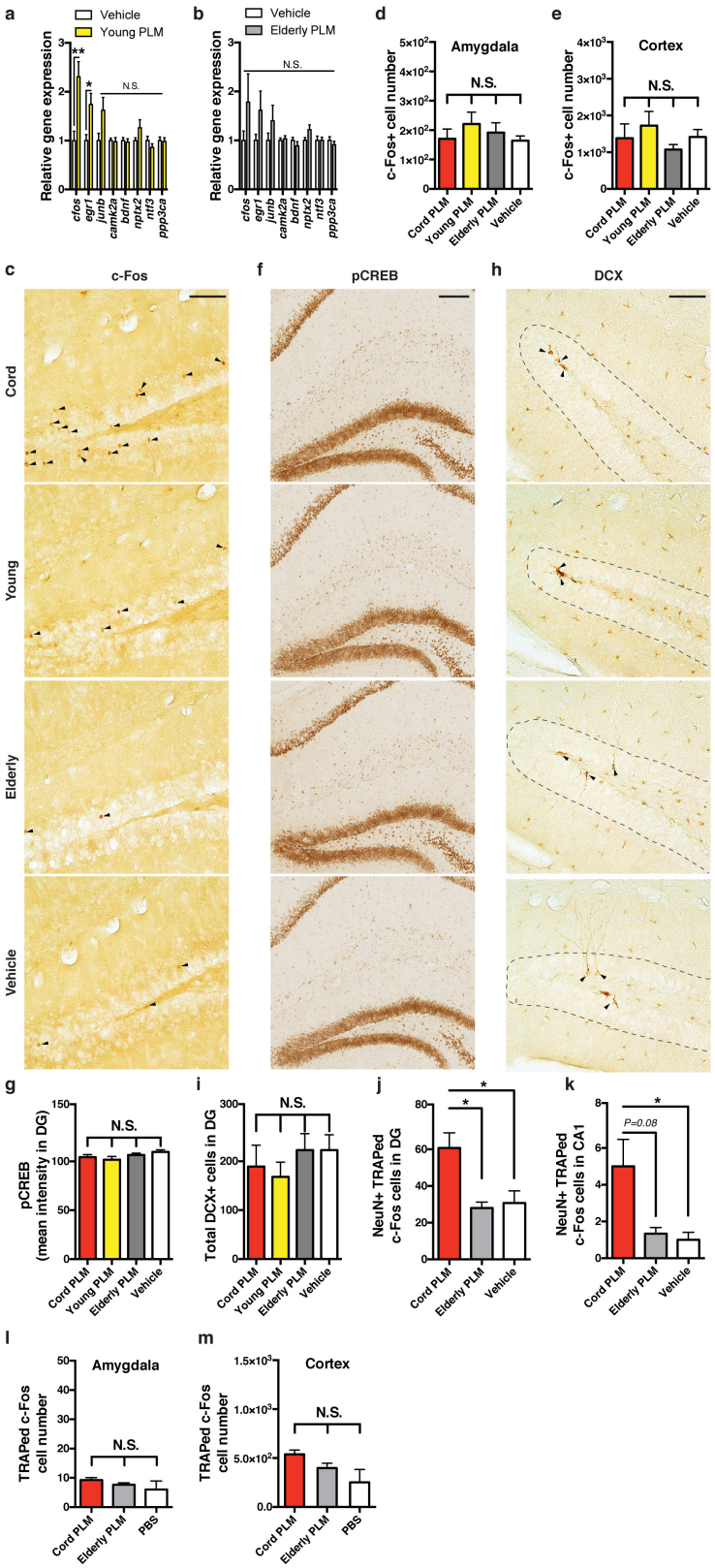

Extended Data Figure 3 | See next page for caption.

Extended Data Figure 3 | Human cord plasma treatment enhances c-Fos expression in the dentate gyrus but does not alter pCREB expression or the number of newborn neurons. a, **b**, Relative gene expression by qPCR for confirmatory plasticity genes after treatment of aged NSG mice with young (**a**; $n = 6$) or elderly (**b**; $n = 7$) human plasma versus vehicle ($n = 7$) (13.9 ± 0.2 months old). **c**, Representative dentate gyrus images from aged NSG mice treated intravenously with human cord ($n = 8$ mice), young ($n = 7$ mice), or elderly ($n = 7$ mice) plasma or vehicle ($n = 7$ mice), highlighting c-Fos-positive cells (arrowheads; scale bar, 100 μm; quantification in Fig. 1e). **d**, **e**, Quantification of c-Fos-positive cells in lateral/basolateral amygdala (**d**) and retrosplenial/motor cortex (**e**) in treated NSG mice. **f**, **g**, pCREB expression (**f**; scale bar, 150 μm) and corresponding pCREB intensity quantification (**g**) in treated NSG mice. **h**, **i**, Newborn neurons visualized by doublecortin antibody staining (**h**; DCX, arrowheads; scale bar, 100 μm) and corresponding quantification (**i**) in treated NSG mice; (for **a**–**g**, 13.9 ± 0.2 months old). **j**, **k**, Quantification of TRAPed c-Fos-activated recombined cells (visualized by TdTomato fluorescence) also expressing the pan-neuronal marker NeuN in dentate gyrus (**j**) and the CA1 subfield of hippocampus (**k**; overall activation/recombination in CA1 was very low) from cord plasma-treated ($n = 4$), elderly plasma-treated ($n = 3$), and vehicle-treated ($n = 4$) TRAP-FOS mice (8–9.5 months old). **l**, **m**, TRAPed c-Fos-activated recombined cells in lateral/basolateral amygdala (**l**) and retrosplenial/motor cortex (**m**) in mice from **j**–**k**; one-way ANOVA with Tukey's post hoc test; $^{*}P < 0.05$, $^{**}P < 0.01$; NS, not significant; mean ± s.e.m.

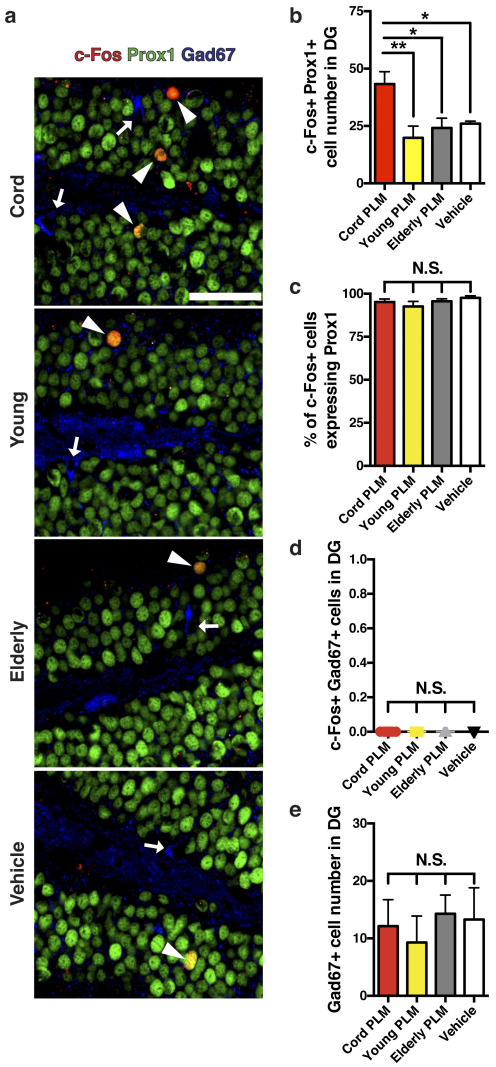

Extended Data Figure 4 | Most c-Fos-expressing cells activated by cord plasma in dentate gyrus are granule cells. a, **b**, Overlap (arrowheads) of c-Fos (red) and prox1 (green), and Gad67-expressing neurons (blue; arrows) in dentate gyrus from cord plasma-treated ($n = 8$), young plasma-treated ($n = 7$), elderly plasma-treated ($n = 7$), and vehicle-treated ($n = 7$) NSG mice by confocal microscopy (**a**) with corresponding counts of c-Fos$^+$prox1$^+$ neurons (**b**; 13.9 ± 0.2 months old; scale bar, $50\,\mu m$). **c**, The proportion of c-Fos-expressing cells quantified in dentate gyrus that were granule cells (prox1$^+$), suggesting that nearly all the c-Fos$^+$ cells detected in dentate gyrus were granule cells. **d**, Quantification of the number of c-Fos$^+$Gad67$^+$ (inhibitory neuron) cells in dentate gyrus from human plasma- and vehicle-treated NSG mice. **e**, Quantification of the number of Gad67$^+$ cells in the dentate gyrus of treated NSG mice. One-way ANOVA with Tukey's post hoc test; $^*P < 0.05$, $^{**}P < 0.01$; NS, not significant; mean $\pm$ s.e.m.

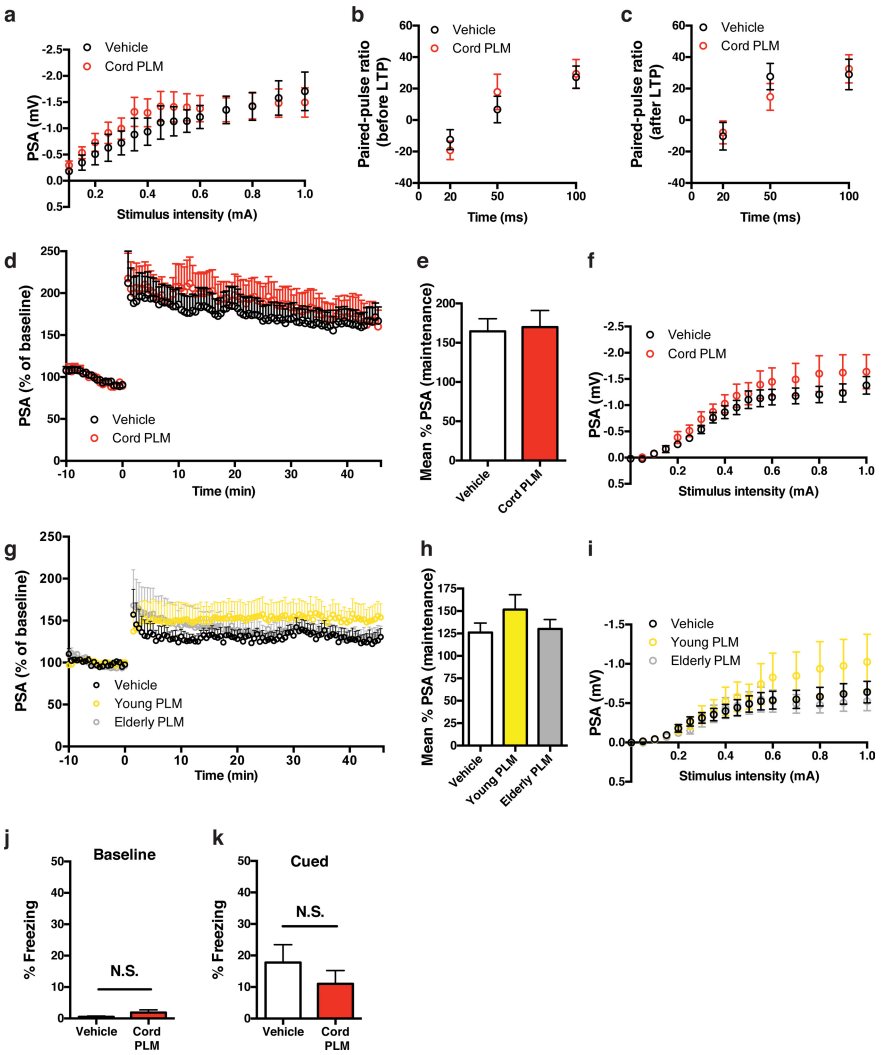

Extended Data Figure 5 | Cord, but not young or elderly plasma, affects LTP in aged NSG hippocampi without altering synaptic strength and paired-pulse facilitation. **a**, Input–output relationship in dentate gyrus synapses from brain slices taken from vehicle- or cord-plasma-treated aged NSG mice ($n = 11$ slices from $n = 5$ cord plasma-treated NSG mice; $n = 12$ slices from $n = 5$ vehicle-treated NSG mice; eight intravenous injections; 11.7 ± 0.2 months old), showing no difference in synaptic strength (basal synaptic transmission). **b**, **c**, Paired-pulse ratio before (**b**) and after (**c**) LTP protocol with various pulse intervals (in **c**, $n = 10$ slices per group were measured). **d**–**f**, Population spike amplitudes recorded in dentate gyrus granule cell layer by perforant path stimulation in slices from vehicle- or cord plasma-treated young NSG mice (**d**) with quantification of LTP maintenance phase (**e**), and input–output relationship (**f**) in dentate gyrus synapses from the slices ($n = 11$ slices per group from $n = 5$ mice per group; eight intravenous injections; 2.5 ± 0.1 months old). **g**–**i**, Population spike amplitudes recorded in dentate gyrus granule cell layer by perforant path stimulation in slices from vehicle, young, or elderly human plasma-treated aged NSG mice (**g**) with quantification of LTP maintenance phase (**h**), and input–output relationship in dentate gyrus synapses (**i**) from the slices ($n = 10$, 11, and 11 slices from 5 mice per group (vehicle-treated, young plasma-treated, and elderly plasma-treated mice, respectively); eight intravenous injections; 12.0 ± 0.1 months old). **j**, **k**, Freezing levels for vehicle-treated ($n = 9$) or cord-plasma-treated ($n = 7$) aged NSG mice during baseline period (**j**) and cued fear-conditioning task (**k**; eight intravenous injections; 12.8 ± 0.2 months old). Student's *t*-test for two-group comparisons; one-way ANOVA for **h**; two-way ANOVA for group × stimulus intensity comparisons (no significant interaction in **a**, **f**, **i**); NS, not significant; mean ± s.e.m.

a

Plasma factor	Protein array changes	Meta-ranking	*d*-score
TIMP2	↓ mouse/human	1†	2.29
NRG1	↓ mouse/human	2	2.28
GRN	↓ mouse/human	3*	2.26
CD46	↓ mouse/human	4	2.23
CCL27	↓ mouse/human	5	2.03
IL9	↓ mouse/human	6	2.03
IL19	↓ mouse/human	7	1.96
EPGN	↓ mouse/human	8	1.88
FGF12	↓ mouse/human	9	1.87
C1orf187	↓ mouse/human	10	1.86
FGF11	↓ mouse/human	11*	1.85
A2M	↓ mouse/human	12*	1.71
TNFRSF21	↓ mouse/human	13	1.48
IL20	↓ mouse/human	14	1.16
CCL18	↓ mouse/human	15	1.12
IL16	↓ mouse/human	16	0.94
NCAM1	↓ mouse/human	17	0.92
NLGN1	↑ parabiosis ↓human	1	1.59
CSF2	↑ parabiosis ↓human	2†	1.57
A2M	↑ parabiosis ↓human	3*	1.55
GDF2	↑ parabiosis ↓human	4	1.49
CD46	↑ parabiosis ↓human	5	1.26
JAG1	↑ parabiosis ↓human	6	1.23
KITLG	↑ parabiosis ↓human	7	1.20
GAS6	↑ parabiosis ↓human	8†	1.18
FGF11	↑ parabiosis ↓human	9*	1.02
GRN	↑ parabiosis ↓human	10*	0.96
CADM4	↑ parabiosis ↓human	11	0.93
ACAN	↑ parabiosis ↓human	12	0.92
CHRD	↑ parabiosis ↓human	13	0.88
CCL27	↑ parabiosis ↓human	14	0.84
IL20	↑ parabiosis ↓human	15	0.83
LUM	↑ parabiosis ↓human	16	0.66

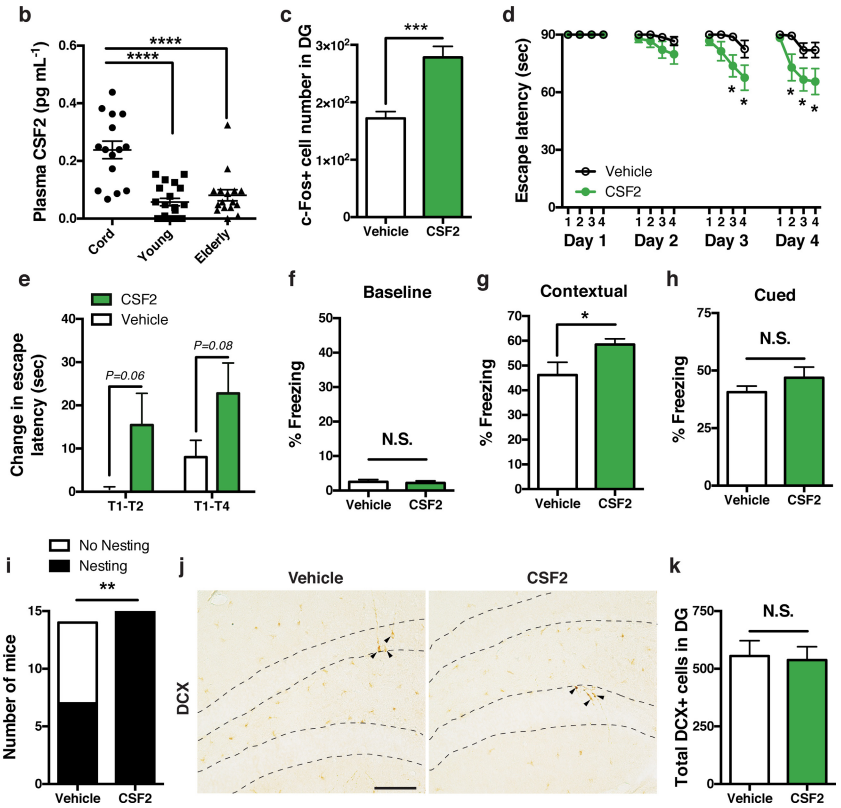

Extended Data Figure 6 | Systemic treatment with CSF2 improves learning and memory in aged mice. a, Table of ranked plasma protein changes from protein microarray experiments. Shown in green are top hits of proteins decreasing in plasma in both mouse ageing (3, 6, 12, 18, 24 months) and human ageing (cord, young, elderly) arrays; shown in red are top hits of proteins increasing in plasma of aged mice sharing young blood (versus aged isochronic), while also decreasing in human ageing (cord, young, elderly) arrays. †Candidates selected for recombinant protein injections in aged mice to examine changes in c-Fos^{+} cell number. *Proteins appearing in both lists. **b**, Scatter plot of ELISA-based quantification of human plasma CSF2 ($n = 15$, 19, 16 subjects (left to right)), consistent with plasma elevations in aged mice sharing young blood via parabiosis by protein microarray. **c**, Number of c-Fos-positive cells in dentate gyrus from aged WT mice treated seven times systemically every other day with 50 μg kg^{-1} (intraperitoneal) recombinant CSF2 ($n = 8$ per group; 21-month-old). **d**, Barnes maze escape latency over 4-day trial time course for separate cohort of aged WT mice (20-month-old) treated systemically (intraperitoneal) eight times every other day with vehicle ($n = 14$) or 50 μg kg^{-1} of recombinant CSF2 ($n = 15$). **e**, Day 4 Barnes maze acquisition rate for indicated trial intervals. **f**–**h**, Baseline freezing levels for the same CSF2- or vehicle-treated cohort in **d** and **e** (**f**), and freezing levels during exposure to previously aversive context (**g**) or during exposure to a new context chamber with training cues (**h**). **i**, Number of treated WT mice from **d**–**h** exhibiting nesting behaviour within 24 h of placing intact nestlet under single-housing conditions. **j**, **k**, Representative dentate gyrus sections stained with doublecortin antibody (DCX, arrowheads; scale bar, 100 μm) in CSF2-treated versus vehicle-treated aged WT mice from **d**–**i** (**j**) and corresponding quantification of total newborn neuron number in dentate gyrus (**k**), suggesting that cognitive changes observed in **d**, **e**, and **g** are probably unrelated to neurogenesis changes. One-way ANOVA with Tukey's post hoc test; two-way repeated-measures ANOVA with Bonferroni's post hoc test for time × group comparisons; Student's *t*-test for two-group comparisons; χ^2 analysis for **i**. *$P < 0.05$, **$P < 0.01$, ****$P < 0.0001$; mean ± s.e.m.

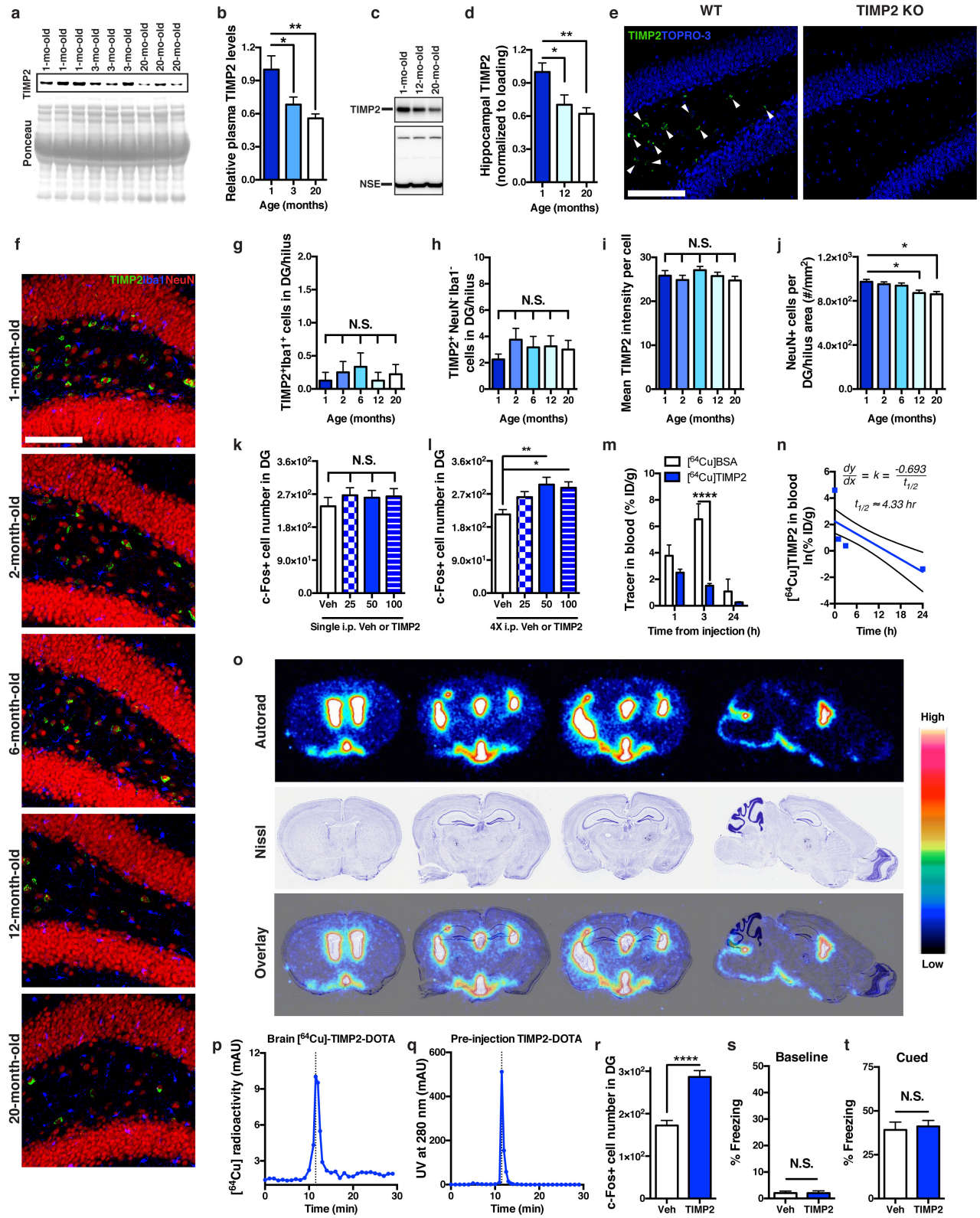

Extended Data Figure 7 | See next page for caption.

Extended Data Figure 7 | TIMP2 decreases early in plasma and hippocampus and enters the CNS following systemic treatment. **a**, **b**, Representative immunoblot detecting TIMP2 from equal volumes of 1-month-old ($n = 8$), 3-month-old ($n = 7$), and 20-month-old ($n = 8$) WT mouse plasma with corresponding Ponceau S stain (**a**) and quantification (**b**). **c**, **d**, Representative immunoblot detecting TIMP2 and neuron-specific enolase loading control from hippocampal lysates (80 μg) from 1-, 12- and 20-month-old WT mice (**c**) with corresponding quantification (**d**; $n = 7$ per group). **e**, Representative confocal microscopy images from WT or TIMP2 KO mice demonstrating specificity of TIMP2 signal (green) in dentate gyrus ($n = 4$ mice per group; 3-month-old male mice; white arrowheads indicate $TIMP2^+$ cells; scale bar, 100 μm). **f**, Representative confocal microscopy images showing TIMP2 (green), Iba1 (blue), and NeuN (red) staining in dentate gyrus/hilus of WT mice at various ages (C57Bl/6; National Institute on Aging colony; 1-month-old ($n = 8$), 2-month-old ($n = 8$), 6-month-old ($n = 6$), 12-month-old ($n = 8$), and 20-month-old mice ($n = 9$); scale bar, 100 μm). **g**, **h**, Quantification of $TIMP2^+Iba1^+$ cells (**g**) or $TIMP2^+$ cells lacking Iba1 or NeuN staining (**h**) in the dentate gyrus/hilus of mice from **f**. **i**, Mean signal intensity per $TIMP2^+$ cell for all counted cells within dentate gyrus/hilus in mice from **f**. **j**, $NeuN^+$ cell counts per dentate gyrus/hilar area in the indicated ages. **k**, **l**, c-Fos-positive cell counts within dentate gyrus from WT mice treated once (**k**) or four times (**l**) with different rTIMP2 doses ($n = 8$ per group; 21-month-old). **m**, ^{64}Cu-labelled BSA and ^{64}Cu-labelled TIMP2 detected in blood of 21-month-old WT mice euthanized at the indicated time points following an injected dose of ^{64}Cu-labelled BSA ($n = 4$ mice per time point ($n = 3$ mice at 24 h)) or ^{64}Cu-labelled TIMP2 ($n = 5$ mice per time point). **n**, First-order elimination kinetics of ^{64}Cu-labelled TIMP2 levels were analysed to approximate its blood half-life (curved line indicates confidence interval). **o**, *Ex vivo* autoradiography assessment of ^{64}Cu-labelled TIMP2 localization in coronal or sagittal (right-most) brain sections from injected mice (top) with corresponding Nissl staining (middle) and ^{64}Cu-labelled TIMP2/Nissl overlay to examine anatomical co-registration with radioactive signal (colour bar indicates radioactive signal from low (black) to high (white); $n = 3$ per group; ~20-month-old WT mice). **p**, Representative analytical high-performance liquid chromatography radioactivity chromatogram from mouse brain homogenates to assess stability of ^{64}Cu-labelled TIMP2 24 h after injection. Dotted line corresponds to retention time of 11.5 min ($n = 2$ per group; ~20-month-old WT mice). **q**, Ultraviolet absorbance at 280 nm measured for TIMP2–DOTA before injection *in vivo*, exhibiting identical retention time as in **m**. **r**, Number of c-Fos^+ cells in dentate gyrus from aged (21-month-old) WT mice treated seven times systemically every other day with vehicle ($n = 8$) or 50 μg kg^{-1} (intraperitoneal) recombinant TIMP2 ($n = 7$). **s**, **t**, Freezing levels for vehicle- or TIMP2-treated aged WT mice during baseline period (**s**) and during cued fear-conditioning task (**t**; $n = 15$ per group; eight intraperitoneal injections; 20-month-old). See Supplementary Fig. 1 for uncropped blot images. One-way ANOVA with Tukey's post hoc test; two-way ANOVA with Bonferroni's post hoc test for group × time comparisons; Student's *t*-test for two-group comparisons. $*P < 0.05$, $**P < 0.01$, $****P < 0.0001$; NS, not significant; mean ± s.e.m.

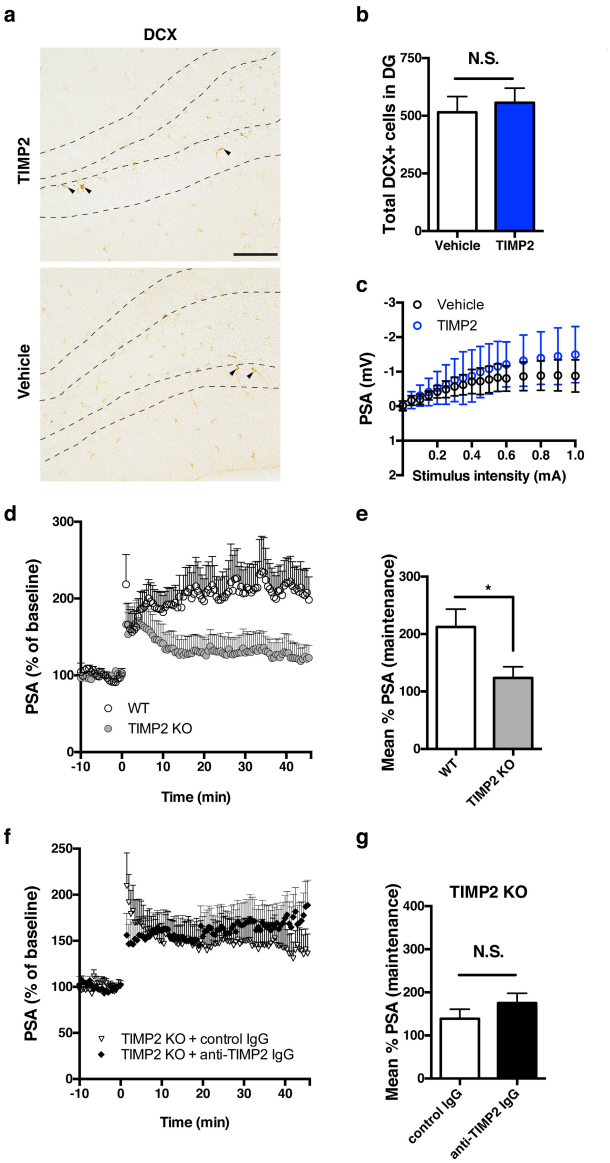

Extended Data Figure 8 | Effect of systemic TIMP2 treatment or whole-body TIMP2 deletion on dentate gyrus synaptic plasticity. **a**, **b**, Representative dentate gyrus sections stained with doublecortin antibody (DCX, arrowheads; scale bar, 100 μm) in vehicle- or TIMP2-treated WT mice (**a**) and corresponding quantification (**b**) of total newborn neuron number in dentate gyrus ($n = 15$ mice per group; 20-month-old). **c**, Input–output relationship in dentate gyrus synapses from hippocampal slices taken from vehicle- or TIMP2-treated WT mice ($n = 10$ slices per group from $n = 5$ mice per group; eight intraperitoneal injections; 20-month-old), showing no difference in synaptic strength (basal synaptic transmission); mean ± s.d. **d**, **e**, Population spike amplitudes recorded in dentate gyrus granule cell layer after perforant path stimulation in slices from TIMP2 KO or WT mice (**d**) and quantification (**e**) of LTP maintenance phase ($n = 10$ slices per group from $n = 5$ mice per group; 2-month-old mice). **f**, **g**, Population spike amplitudes recorded in dentate gyrus granule cell layer after perforant path stimulation in TIMP2 KO slices incubated with the indicated *ex vivo* treatments (**f**) and quantification (**g**) of LTP maintenance phase ($n = 8$ slices (control IgG incubations) from $n = 4$ mice; $n = 10$ slices (anti-TIMP2 IgG incubations) from $n = 5$ mice; 2- to 3-month-old sex-matched mice); Student's *t*-test for two-group comparisons; $^*P < 0.05$; NS, not significant; mean ± s.e.m.

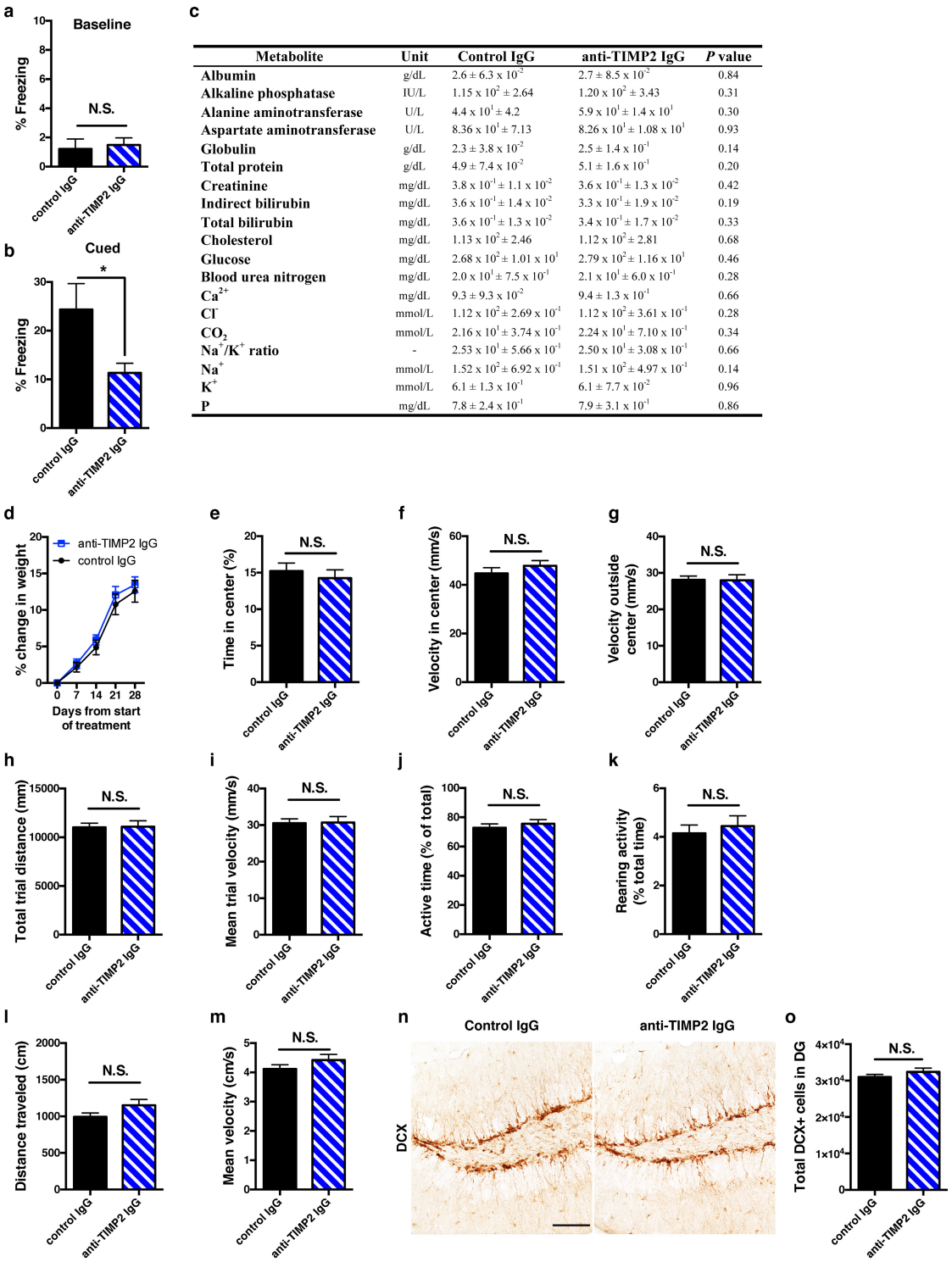

Metabolite	Unit	Control IgG	anti-TIMP2 IgG	*P* value
Albumin	g/dL	$2.6 \pm 6.3 \times 10^{-2}$	$2.7 \pm 8.5 \times 10^{-2}$	0.84
Alkaline phosphatase	IU/L	$1.15 \times 10^{2} \pm 2.64$	$1.20 \times 10^{2} \pm 3.43$	0.31
Alanine aminotransferase	U/L	$4.4 \times 10^{1} \pm 4.2$	$5.9 \times 10^{1} \pm 1.4 \times 10^{1}$	0.30
Aspartate aminotransferase	U/L	$8.36 \times 10^{1} \pm 7.13$	$8.26 \times 10^{1} \pm 1.08 \times 10^{1}$	0.93
Globulin	g/dL	$2.3 \pm 3.8 \times 10^{-2}$	$2.5 \pm 1.4 \times 10^{-1}$	0.14
Total protein	g/dL	$4.9 \pm 7.4 \times 10^{-2}$	$5.1 \pm 1.6 \times 10^{-1}$	0.20
Creatinine	mg/dL	$3.8 \times 10^{-1} \pm 1.1 \times 10^{-2}$	$3.6 \times 10^{-1} \pm 1.3 \times 10^{-2}$	0.42
Indirect bilirubin	mg/dL	$3.6 \times 10^{-1} \pm 1.4 \times 10^{-2}$	$3.3 \times 10^{-1} \pm 1.9 \times 10^{-2}$	0.19
Total bilirubin	mg/dL	$3.6 \times 10^{-1} \pm 1.3 \times 10^{-2}$	$3.4 \times 10^{-1} \pm 1.7 \times 10^{-2}$	0.33
Cholesterol	mg/dL	$1.13 \times 10^{2} \pm 2.46$	$1.12 \times 10^{2} \pm 2.81$	0.68
Glucose	mg/dL	$2.68 \times 10^{2} \pm 1.01 \times 10^{1}$	$2.79 \times 10^{2} \pm 1.16 \times 10^{1}$	0.46
Blood urea nitrogen	mg/dL	$2.0 \times 10^{1} \pm 7.5 \times 10^{-1}$	$2.1 \times 10^{1} \pm 6.0 \times 10^{-1}$	0.28
Ca^{2+}	mg/dL	$9.3 \pm 9.3 \times 10^{-2}$	$9.4 \pm 1.3 \times 10^{-1}$	0.66
Cl^{-}	mmol/L	$1.12 \times 10^{2} \pm 2.69 \times 10^{-1}$	$1.12 \times 10^{2} \pm 3.61 \times 10^{-1}$	0.28
CO_2	mmol/L	$2.16 \times 10^{1} \pm 3.74 \times 10^{-1}$	$2.24 \times 10^{1} \pm 7.10 \times 10^{-1}$	0.34
Na^{+}/K^{+} ratio	-	$2.53 \times 10^{1} \pm 5.66 \times 10^{-1}$	$2.50 \times 10^{1} \pm 3.08 \times 10^{-1}$	0.66
Na^{+}	mmol/L	$1.52 \times 10^{2} \pm 6.92 \times 10^{-1}$	$1.51 \times 10^{2} \pm 4.97 \times 10^{-1}$	0.14
K^{+}	mmol/L	$6.1 \pm 1.3 \times 10^{-1}$	$6.1 \pm 7.7 \times 10^{-2}$	0.96
P	mg/dL	$7.8 \pm 2.4 \times 10^{-1}$	$7.9 \pm 3.1 \times 10^{-1}$	0.86

Extended Data Figure 9 | Systemic TIMP2 neutralization alters spatial memory but not activity or general health parameters. a, **b**, Baseline freezing levels (**a**) and cued fear-conditioning freezing levels (**b**) in young WT mice treated with anti-TIMP2 IgG or control IgG (60 μg kg^{-1}) for 2 weeks ($n = 15$ per group; 2-month-old). **c**, **d**, Serum metabolite measurements (**c**) and weekly weights (**d**) to assess general health and organ function in young WT mice treated for ~4 weeks with anti-TIMP2 IgG or control IgG. **e**, **f**, Proportion of trial time spent in centre (**e**) and velocity in centre (**f**) during open-field assessment of anxiety-like behaviour in the treated mice. **g**–**i**, Velocity in zone outside the centre (**g**), total trial distance (**h**), and mean trial velocity (**i**; centre and outside) during open-field testing. **j**–**m**, General activity (**j**), rearing activity (**k**), distance travelled (**l**), and mean trial velocity (**m**)—all monitored by SMARTCage beam-breaks in a home cage for the treated mice. **n**, **o**, Quantification of total newborn neuron number in dentate gyrus (**n**) with corresponding representative dentate gyrus sections stained with doublecortin antibody (**o**; DCX, arrowheads; scale bar, 100 μm) in control IgG- or anti-TIMP2 IgG-treated young mice; For **d**–**o**, $n = 15$ mice per group; 2.5-month-old; in **c**, one serum sample in each group was not submitted for metabolite testing owing to a high degree of haemolysis in these two samples; Student's *t*-test; $^{*}P < 0.05$; NS, not significant; mean ± s.e.m.

a

Plasma factor	↑ or ↓ in TIMP2 KO	Significance level
TIMP2	↓	****
TIMP2'	↓	****
SPP1	↑	****
DKK4	↓	****
C6	↑	***
HP	↑	**
FGF16	↑	**
NOV	↑	**
CCL5	↑	**
FGF7	↑	**
IGFBP6	↓	**
IL1RAPL1	↑	**
FGF5	↑	**
FGF23	↑	**
TNFSF10	↑	**
NGFR	↑	*
C1R	↑	*
FGF17	↑	*
C5	↑	*
BMP10	↓	*
GDF1	↑	*
IL1A	↑	*
TNFSF18	↑	*
FGF6	↑	*
CXCL16	↑	*
FRZB	↑	*
TNFSF9	↑	*
MMP2	↓	*
CER1	↑	*
CCL28	↑	*
TNFAIP6	↑	*
CCL1	↑	*
CXCL5	↑	*
XCL1	↑	*

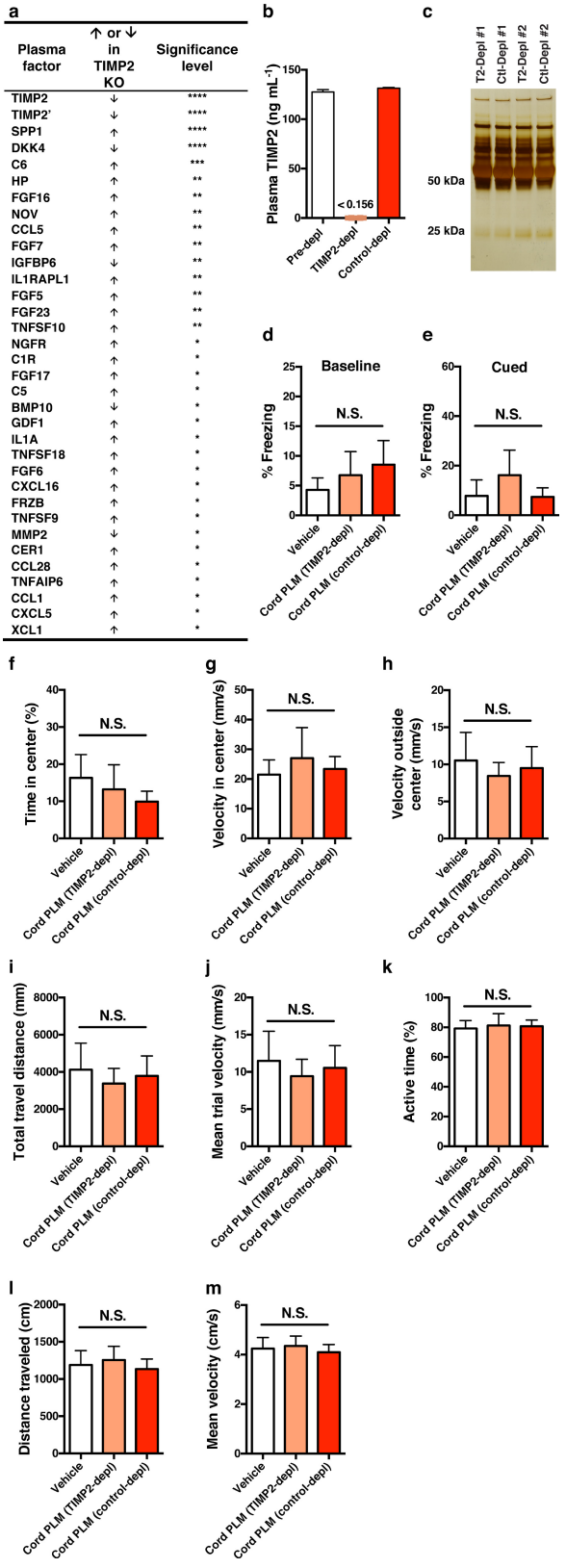

Extended Data Figure 10 | TIMP2 is critical for several cognitive benefits of cord plasma independent of activity behaviour. a, Table of significant changes (ranked by effect size) in the relative level of plasma proteins in young (3-month-old) TIMP2 KO ($n = 13$) versus WT ($n = 9$) mice measured by customized protein microarray. The first two entries represent two different antibodies against TIMP2. **b**, Mean TIMP2 concentrations determined by ELISA (±s.d. for technical replicates) for cord plasma pre-depletion, or cord plasma after TIMP2 or control depletion. **c**, Silver-stained gel loaded with elution from beads used for TIMP2 (T2) or control (ctl) depletion. '#1' and '#2' reflect replicate plasma aliquots from the depletion process (see Supplementary Fig. 1 for uncropped gel image). **d**, **e**, Baseline freezing levels (**d**) and cued fear-conditioning freezing levels (**e**) in aged NSG mice (13.8 ± 0.1 months old) given eight intravenous injections of vehicle ($n = 10$), TIMP2-depleted cord plasma ($n = 8$), and IgG control-depleted cord plasma ($n = 9$). **f**, **g**, Proportion of trial time spent in centre (**f**) and velocity in centre (**g**) during open-field assessment of anxiety-like behaviour in the treated mice. **h**–**j**, Velocity in zone outside the centre (**h**), total travel distance (**i**), and mean trial velocity (**j**; centre and outside) during open-field testing. **k**–**m**, General activity (**k**), distance travelled (**l**), and mean trial velocity (**m**) by SMARTCage beam-break monitoring for the treated mice. One-way ANOVA with Tukey's post hoc test; Student's *t*-test for WT versus TIMP2 KO comparisons with $q < 0.15$; $^{*}P < 0.05$, $^{**}P < 0.01$, $^{***}P < 0.001$, $^{****}P < 0.0001$; NS, not significant; mean ± s.e.m.